

Benchmarking Adversarial Robustness and Adversarial Training Strategies for Object Detection

Alexis Winter^{1*†}, Jean-Vincent Martini^{1†}, Romaric Audigier¹,
Angelique Loesch¹, Bertrand Luvison¹

¹Université Paris-Saclay, CEA, List, F-91191, Palaiseau, France.

^{*}Corresponding author(s). E-mail(s): alexis.winter@cea.fr;

[†]These authors contributed equally to this work.

Abstract

Object detection models are critical components of automated systems, such as autonomous vehicles and perception-based robots, but their sensitivity to adversarial attacks poses a serious security risk. Progress in defending these models lags behind classification, hindered by a lack of standardized evaluation. It is nearly impossible to thoroughly compare attack or defense methods, as existing work uses different datasets, inconsistent efficiency metrics, and varied measures of perturbation cost. This paper addresses this gap by investigating three key questions: (1) How can we create a fair benchmark to impartially compare attacks? (2) How well do modern attacks transfer across different architectures, especially from Convolutional Neural Networks to Vision Transformers? (3) What is the most effective adversarial training strategy for robust defense? To answer these, we first propose a unified benchmark framework focused on digital, non-patch-based attacks. This framework introduces specific metrics to disentangle localization and classification errors and evaluates attack cost using multiple perceptual metrics. Using this benchmark, we conduct extensive experiments on state-of-the-art attacks and a wide range of detectors. Our findings reveal two major conclusions: first, modern adversarial attacks against object detection models show a significant lack of transferability to transformer-based architectures. Second, we demonstrate that the most robust adversarial training strategy leverages a dataset composed of a mix of high-perturbation attacks with different objectives (e.g., spatial and semantic), which outperforms training on any single attack.

Keywords: Object Detection, Adversarial Robustness, Adversarial Attacks, Benchmark

Acknowledgments

Funded by the European Union. Views and opinions expressed are however those of the author(s) only and do not necessarily reflect those of the European Union nor the European Commission. Neither the European Union nor the granting authority can be held responsible for them. This work was supported under the EDF Project FaRADAI (grant number 101103386). This work was made possible by the FactoryIA supercomputer (funded by the Ile-de-France Regional Council). This work was supported by a State grant managed by the French National Research Agency, Agence Nationale de la Recherche, under "France 2030" (grant reference "ANR-22-PECY-0011", within the framework of the "COMPROMIS" project).

1 Introduction

Object detectors are central to the deployment of vision systems in open-world environments, yet ensuring their trustworthiness remains a critical challenge as they remain highly vulnerable to adversarial attacks (Amirkhani, Karimi, & Banitalebi-Dehkordi, 2023; Nguyen et al., 2025). In machine learning, adversarial samples are inputs formed by applying specific perturbations to a clean sample that cause a model to produce an incorrect output with high confidence (Goodfellow, Shlens, & Szegedy, 2015). In object detection, adversarial attacks generate perturbations that alter the input images, making detectors ineffective and leading to incorrect predictions which pose a major security threat in applications like autonomous driving, video surveillance, and medical imaging (Amirkhani et al., 2023; Nguyen et al., 2025). Understanding such attacks and improving the robustness of our detectors has therefore become a key research topic to overcome this challenge.

While adversarial robustness has been well studied for classification in recent years (Chakraborty, Alam, Dey, Chattopadhyay, & Mukhopadhyay, 2021; Costa, Roxo, Proen  a, & Inacio, 2024; Miller, Xiang, & Kesidis, 2020), progress in other domains such as deep metric learning (Bai, Li, Zhou, Li, & Torr, 2020; Boumiot, Audigier, & Loesch, 2020; Gong et al., 2024) and object detection is far more limited. This lag is due to two primary issues: the task's inherent complexity and a lack of standardized evaluation. Unlike classification, where an attack's success is a binary outcome, an attack on an object detector can succeed in multiple ways: it can cause an object to go undetected, change its predicted class label, or alter the coordinates of its bounding box (Ding et al., 2024; H. Li et al., 2024; Nezami, Chaturvedi, Dras, & Garain, 2021). This multi-objective failure space makes both designing attacks and evaluating defenses a challenging task. A wide variety of attack strategies have emerged for all these different objectives, from imperceptible perturbations that are invisible to the human eye (Cai, Tan, & Asif, 2023; Cai, Xie, et al., 2022), to physical patch attacks that add a visible artifact to the scene (H. Huang, Chen, Chen, Wang, & Zhang, 2023; X. Liu, Yang, Song, Li, & Chen, 2018). More critically, the field lacks any standardized evaluation. Existing surveys (Amirkhani et al., 2023) provide excellent taxonomies and recent research like (Nguyen et al., 2025) attempts a large-scale comparison, but their work highlights, the difficulty of comparing different attack or defense methodologies and the need for standard evaluation. Even among digital, non-patch-based attacks, existing work uses different datasets and efficiency metrics aligned with their respective objectives (e.g., mAP drop vs. attack success rate). Perturbation constraints are not applied in the same way even though most methods use Lebesgue norms (Cai, Xie, et al., 2022; Ding et al., 2024), and methods often require varying degrees of information regarding the target model from full white-box access (Ding et al., 2024) to query-based grey-box settings (Cai et al., 2023). As detailed in Section 2.5, this fragmentation makes it impossible to assess the true state of the art or identify which methods are genuinely robust.

To address these gaps, we first introduce a critical survey and a new unified benchmark framework for digital, non-patch-based attacks. We then conduct extensive experiments on SOTA attacks, a wide range of detectors, and multiple adversarial training configurations. Our main contributions are as follows:

- We analyze the landscape of adversarial attacks to identify and categorize the most effective methodologies. This analysis exposes the fragmentation of the field, highlighting the disparate datasets, metrics, and perturbation constraints that make comparisons impossible.
- Based on our findings, we propose a unified benchmark focused on digital, non-patch-based attacks. This framework uses specialized metrics (AP_{loc} and CSR) to disentangle localization and classification errors, and two perceptual metrics ($LPIPS$, L_2) to enable fair comparisons of attack efficiency and transferability.
- We provide an analysis of cross-architectural transferability, revealing a robustness gap where modern attacks fail to transfer to modern transformer-based detectors like DINO.
- We demonstrate that training on a mix of high-perturbation attacks with complementary objectives (e.g., spatial and semantic) achieves greater robustness than training on any single attack.

2 Landscape Analysis: Taxonomy, Method Review and Evaluation Gaps

2.1 Preliminaries and terminology

2.1.1 Formal definition of adversarial examples

Adversarial examples are crafted to fool Deep Neural Networks by introducing small perturbations that lead to incorrect predictions. Formally, given a trained model with parameters θ , an input image x , and its ground-truth label y , the standard training objective is to find parameters θ that *minimize* a loss function $\mathcal{L}(x, \theta, y)$. In contrast, an adversarial attack seeks to find a small perturbation δ that *maximizes* this loss, thereby inducing a wrong prediction:

$$\max_{\delta \in \Delta} \mathcal{L}(x + \delta, \theta, y)$$

Here, Δ denotes the set that constrains the perturbations to ensure they remain limited in size. The most prevalent choice is the ℓ_∞ -ball, which limits the maximum change for any single pixel:

$$\Delta = \{\delta \mid \|\delta\|_\infty \leq \epsilon\}$$

where ϵ represents the perturbation budget, i.e., the maximum allowable change in pixel intensity.

For targeted attacks, the goal is not to cause a mistake, but to force the model to predict a specific target label y_{target} . This is achieved by optimizing a contrastive objective that pushes the model's prediction away from the true label and towards the target label:

$$\max_{\delta \in \Delta} (\mathcal{L}(x + \delta, \theta, y) - \mathcal{L}(x + \delta, \theta, y_{target}))$$

The resulting adversarial example is defined as $x^* = x + \delta$. While the loss function \mathcal{L} is generic, in modern object detectors it is typically factorized into three main terms: classification, localization, and objectness.

Classification Loss (\mathcal{L}_{cls}): Measures the error in predicting the class of a detected object, for example, using cross-entropy.

$$\mathcal{L}_{\text{cls}} = - \sum_{i \in \mathcal{O}} \sum_{c=1}^C y_i^{(c)} \log \hat{p}_i^{(c)}$$

Here, \mathcal{O} is the set of anchors matched to ground-truth objects, C is the number of classes, $y_i^{(c)}$ is the binary ground-truth indicator, and $\hat{p}_i^{(c)}$ is the predicted probability that object i belongs to class c .

Localization Loss (\mathcal{L}_{loc}): Measures the error between the predicted bounding box coordinates (\hat{b}) and the ground-truth box (b), for example, using the Smooth L1 loss.

$$\mathcal{L}_{\text{loc}} = \sum_{i \in \mathcal{O}} \sum_{j \in \{x, y, w, h\}} \text{SmoothL1}(b_i^{(j)} - \hat{b}_i^{(j)}) \quad \text{where} \quad \text{SmoothL1}(z) = \begin{cases} 0.5z^2 & \text{if } |z| < 1 \\ |z| - 0.5 & \text{otherwise} \end{cases}$$

where j iterates over the bounding box parameters: center coordinates (x, y), width (w), and height (h).

Objectness Loss (\mathcal{L}_{obj}): Measures the error in determining whether a given bounding box contains an object, for example, using binary cross-entropy.

$$\mathcal{L}_{\text{obj}} = - \sum_{i=1}^N \left[y_i^{\text{obj}} \log \hat{o}_i + (1 - y_i^{\text{obj}}) \log (1 - \hat{o}_i) \right]$$

where N is the total number of candidate boxes, $y_i^{\text{obj}} \in \{0, 1\}$ indicates the presence of an object, and \hat{o}_i is the predicted objectness confidence score.

2.1.2 A taxonomy of attacks and models for object detection

Attacks and models can be classified based on their characteristics, context, and intent (see Figure 1). The outcomes of attacks, i.e., the types of impact that the adversarial perturbation has on the predictions of the target detector, are then used to classify the attacks in our survey.

Attack environment: Digital: Attacks that directly distort the input image of the target detector. This is by far the most common type of attack in the literature (Cai et al., 2023; Ding et al., 2024; Xie et al., 2017), applicable to any suitable existing dataset.

Physical: Attacks that involve modifying or adding real-world objects (Xu et al., 2020) to the scene captured by a camera to fool the detector. They are usually an extension of digital attacks, especially for those using a patch that can be printed or projected (D.Y. Yang et al., 2018).

Attack locality: Entire Image: The perturbations are not restricted to any part of the image. These attacks usually aim to remain "imperceptible" and are often

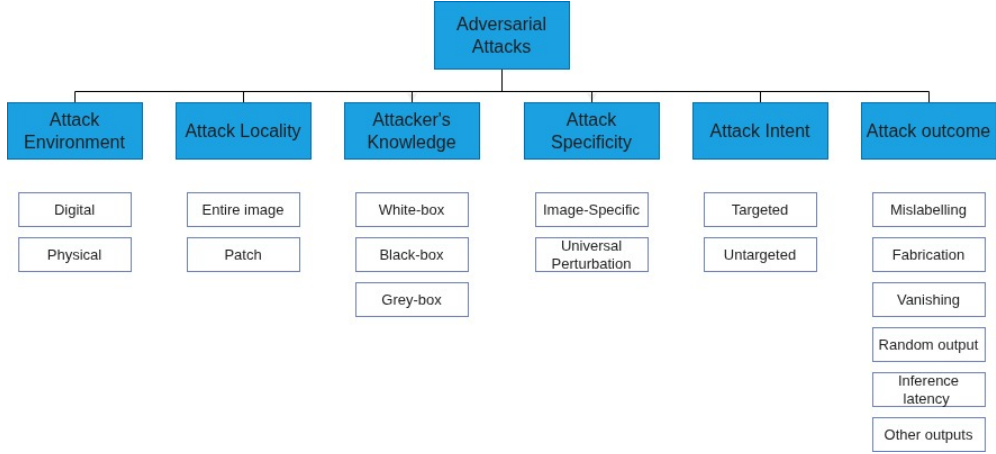


Fig. 1 A taxonomy of adversarial attacks in object detection.

constrained by a perturbation budget limit to control the alteration (Cai et al., 2023; Ding et al., 2024; Xie et al., 2017).

Patch: The effects of these attacks are restricted to a specific area. Some attacks allow multiple patches on one image or patches with different dimensions. These patches are generally not intended to be imperceptible, but some are, such as PRFA (Liang, Wu, Fan, Wei, & Cao, 2021), Imperceptible background patches (Y. Li, Bian, & Lyu, 2018) or RPAttack (H. Huang et al., 2021).

Attacker's knowledge: **White-box attacks:** In a white-box attack scenario, the attacker has complete knowledge of the target model, including the network architecture, the parameter values, the training procedure and the training dataset. Therefore, specific attacks can be designed to maximize the effects on the target (Chow et al., 2020).

Black-box attacks: In a black-box attack scenario, the attacker does not have knowledge of the target model. They are limited to querying the model with images and observing the resulting predictions. To overcome this, many methods rely on transferability: some attacks utilize a known "surrogate" model to generate perturbations that target the unknown "victim" (Ding et al., 2024). Others employ an ensemble of surrogate models to ensure the perturbation remains effective across different types of detectors, such as CAA (Cai, Xie, et al., 2022) or EBAD (Cai et al., 2023).

Grey-box attacks: A grey-box attack scenario falls between white-box and black-box attacks. In this setting, the attacker only has some knowledge about the target model. For example, only the network architecture may be known, but not the training dataset or the parameter values. This additional incomplete information can enable more effective attacks than pure black-box methods (Cai et al., 2023).

Specificity: **Image-specific:** The attack applies an optimized perturbation which is different for each image. This is the most common paradigm among existing

attacks (Cai et al., 2023; Ding et al., 2024; Xie et al., 2017).

Universal perturbation: The same perturbation is applied to every image in the dataset. This process requires a training dataset to generate the perturbation, usually with a distribution close to the test dataset. Universal attacks are generally more generic, yet less effective than image-specific ones. Examples include U-DOS (D. Li, Zhang, & Huang, 2021) or PhantomSponges (Shapira, Zolfi, Demetrio, Biggio, & Shabtai, 2023).

Intent: Targeted: Usually associated with mislabeling attacks such as EBAD (Cai et al., 2023). In a targeted attack, the attacker can choose which class will be predicted after applying the perturbation.

Untargeted: The attacker does not specify a target class for the attack. All random output attacks are considered non-targeted (Ding et al., 2024).

Outcome: Object mislabeling: A mislabeling attack perturbs the image so that the model predicts the wrong class for one or more objects present (Cai et al., 2023; Cai, Xie, et al., 2022).

Object fabrication: A fabrication attack is designed to make the model detect non-existent objects in the input image (D. Wang et al., 2021). Sometimes, it can be done with the specific intention of preserving the detection of existing objects, as with PhantomSponges (Shapira et al., 2023).

Object vanishing: A vanishing attack aims to erase one or multiple objects from the model predictions (Guesmi, Bilasco, Shafique, & Alouani, 2024; Y. Zhang et al., 2023).

Random output: A random attack alters the images so that the predictions of the model are different from the ground-truths. There is no specific intent for the result; some objects may vanish, be fabricated, and be mislabeled (Ding et al., 2024).

Inference latency: The purpose of these attacks is to increase the target model's inference time. This is more of an additional effect and is not a common type of attack. As an example, PhantomSponges causes inference latency in addition to having an object fabrication outcome (Shapira et al., 2023).

Other outputs: This category encompasses attacks whose results do not fit into the outcomes mentioned above. For example, ShiftAttack (H. Li et al., 2024) which only shifts the predicted bounding boxes, or attacks that can be used in several configurations for different purposes. Examples include TOG, which can be used as a random, vanishing, fabrication, or mislabeling attack with different constraints of locality and specificity (Chow et al., 2020), or ADC, which can be a mislabeling, vanishing, or fabrication attack (Yin et al., 2022).

An example of an inference result for each outcome is shown in Figure 2.

2.1.3 Other definitions

Transferability: The capacity of a perturbation initially crafted for one model to remain effective against another model or in different configurations and situations. Transferability can be assessed cross-model, cross-backbone, cross-dataset, cross-domain, etc. It is often evaluated in grey-box or black-box settings (Cai et al., 2023;

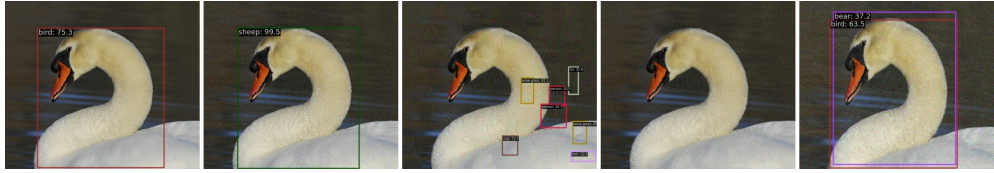


Fig. 2 Inference results for different attack outcomes. From left to right: clean image, object mislabeling attack (EBAD (Cai et al., 2023)), random output attack (OSFD (Ding et al., 2024)), object vanishing attack, and object fabrication attack (PhantomSponges (Shapira et al., 2023)).

Cai, Xie, et al., 2022).

Attacked detector types: **One-stage:** A one-stage detector directly predicts bounding boxes and class labels in a single pass, typically favoring speed. **Anchor-based one-stage:** These use predefined anchor boxes from which final predictions are refined. Examples include early YOLO versions like YOLOv4 (Bochkovskiy, Wang, & Liao, 2020), SSD (W. Liu et al., 2016), and RetinaNet (Lin, Goyal, Girshick, He, & Dollar, 2017). **Anchor-free one-stage:** These directly predict object properties, like center points and dimensions, without predefined anchors, simplifying the pipeline. Examples include FCOS (Tian, Shen, Chen, & He, 2019), CenterNet (Duan et al., 2019), and recent YOLO versions (e.g., YOLOX (Ge, Liu, Wang, Li, & Sun, 2021)). This also covers transformer-based detectors like DETR (Carion et al., 2020) and Deformable-DETR (Zhu et al., 2021), which directly predict objects.

Two-stage: A two-stage detector first generates region proposals and then classifies them, usually prioritizing accuracy over speed. **Anchor-based two-stage:** These primarily use a Region Proposal Network (RPN) to generate proposals based on predefined anchor boxes, refined in a second stage. Examples are Faster R-CNN (Ren, He, Girshick, & Sun, 2015), Cascade R-CNN (Cai & Vasconcelos, 2018), or Libra R-CNN (Pang et al., 2019). **Anchor-free two-stage:** Less common than anchor-based for the two-stage paradigm, this approach involves generating initial region proposals without using predefined anchors and then refining the results. Examples in this category include Sparse R-CNN (P. Sun et al., 2021) and QueryDet (C. Yang, Huang, & Wang, 2022).

2.2 A review of adversarial attacks

Unlike attacks on image classification, object detection attacks are more complex due to the multi-objective nature of the task, involving both object localization and classification. These attacks can be broadly categorized based on their intended outcome.

2.2.1 Object mislabeling

Inspired by classification attack methods, *Dense Adversary Generation (DAG)* is one of the first attacks to target object detection using a gradient-based optimization process (Xie et al., 2017). Focusing on more specific object detection applications,

ShapeShifter (S.-T. Chen, Cornelius, Martin, & Chau, 2018) can generate disturbed "stop" signs that are mis-predicted, highlighting vulnerabilities in autonomous driving vehicles. *Universal Physical Camouflage Attacks* (L. Huang et al., 2020) create patterns applied to people's clothes, thus deceiving the target detector towards the desired class. *Pick-Object Attack* (Nezami et al., 2021) allows for more precise disruptions by targeting only one object per image to change its class. Later attacks also use and alter the context of objects in images. Examples are *Zero-Query Transfer Attacks (ZQA)* (Cai, Rane, et al., 2022), designed specifically for black-box applications, and *Targeted context attack* (C. Sun, Zhang, Han, & Sun, 2024) that focuses on altering the context information of objects by adding a context classification network which brings the original context information closer to the target's contextual information. A key limitation of many methods is their poor transferability in a black-box setting, which has been improved in the two following methods. *Context-Aware Transfer Attack (CAA)* (Cai, Xie, et al., 2022) also leverages contextual dependencies such as object co-occurrence, relative positions while using an ensemble of surrogate models to achieve high transferability. *Ensemble-based Black-box Attacks on Dense Prediction (EBAD)* (Cai et al., 2023) is another ensemble-based attack that optimizes the contribution of each surrogate model for perturbation creation to maximize black-box success.

2.2.2 Object vanishing

Many attacks have been designed to make objects disappear. Several methods aim to make people vanish from detectors such as *Invisible Cloak* (D.Y. Yang et al., 2018), *Adversarial T-shirt* (Xu et al., 2020), *Patches to attack person detection* (Thys, Van Ranst, & Goedeme, 2019) and *FB Invisible cloak* (Z. Wu, Lim, Davis, & Goldstein, 2020). They involve patterns on clothing as well as printable patches. Other patch attacks have been developed for objects other than people. *Contextual Adversarial Patches* (Saha, Subramanya, Patil, & Pirsiavash, 2020) uses spatial context elements to fool the detector with a patch that does not overlap with objects, and *Diffused Patch Attack (DPAttack)* (S. Wu, Dai, & Xia, 2020), a diffused asteroid-shaped or grid-shaped patch that only changes a small number of pixels to fool detectors. Recently, *Transfer-based Self-Ensemble Attack (T-SEA)* (H. Huang et al., 2023) locates every target object from the images with a white-box detector and attaches adversarial patches to their center. *Adversarial Art (AdvART)* (Guesmi et al., 2024) generates semantically coherent patches that attack object detectors. By enforcing semantic constraints, it outperforms methods based on Generative Adversarial Networks (GANs), making the patch more effective and realistic.

For attacks affecting the entire image, *Evaporate Attack* (Y. Wang, Tan, Zhang, Zhao, & Kuang, 2020) combines genetic algorithm and particle swarm optimization to target both region-based and regression-based object detectors. Similarly, *Contextual Adversarial Attack (CAP)* (H. Zhang, Zhou, & Li, 2020) damages context information to achieve high transferability performance and *Universal Dense Object Suppression (U-DOS)* generates universal perturbations while remaining highly effective in making predictions disappear (D. Li et al., 2021). As for patch-based attacks, *Refined Patch Attack (RPAttack)* (H. Huang et al., 2021) only affects a few pixels of

the object and *Naturalistic Physical Adversarial Patch* (Y.-C.-T. Hu et al., 2021) generates natural-looking adversarial patches that remain visually inconspicuous using GAN-based optimization. In more specific applications, *Adversarial Texture* (Z. Hu et al., 2022) applies patterns to people's clothes to fool person detectors even under different viewing angles and deformations. *Patch Attack Against Unmanned Aerial Vehicles (UAV)* (Shrestha, Pathak, & Viegas, 2023) uses patches placed on cars to hide them from detectors. The most recent vanishing attack that does not involve a patch is *Adversarial Semantic Contours (ASC)* (Y. Zhang et al., 2023). Instead of modifying the entire image, ASC only perturbs a small number of pixels, around the object's contour, to fool the detector and make the object disappear.

2.2.3 Object fabrication

Fabrication attacks often target the non-maximum suppression (NMS) step, which eliminates redundant bounding boxes around the same object, in order to create non-existent objects. For example, *Daedalus* (D. Wang et al., 2021) attacks the NMS by compressing the dimensions of the bounding boxes such that detections do not overlap and creates extremely dense false positives. *PhantomSponges* (Shapira et al., 2023) generates a universal adversarial perturbation that also targets NMS. This perturbation causes inference latency by adding non-existent objects that overload the NMS. For patch-based attacks, *Patch-based False Positive creation* (Tang, Yao, Jiang, Zhao, & Sun, 2024) generates a series of patches, each designed to cause the detection of a non-existent object of a different class.

2.2.4 Random output

Some attacks do not have a specific outcome objective, such as *Robust Adversarial Perturbation (R-AP)* (Y. Li, Tian, Chang, Bian, & Lyu, 2018) that aims to disturb the predictions of the Region Proposal Network. Inspired by the mislabeling attack DAG (see Section 2.2.1), *Unified and Efficient Adversary (UEA)* (Wei, Liang, Chen, & Cao, 2019) optimizes a total loss function which is a combination of a GAN loss and the DAG attack loss. The GAN framework generates perturbations that are effective and visually similar to the original images. For patch-based attacks, *DPatch* (X. Liu et al., 2018) produces location independent patches, while *Imperceptible background patches* (Y. Li, Bian, & Lyu, 2018) applies several imperceptible patches in the background of images. *Parallel Rectangle Flip Attack* (Liang et al., 2021) also uses imperceptible patches around objects placed at critical points, avoiding suboptimal detection near the attacked region. *Relevance Attack on Detectors (RAD)* (S. Chen, He, Huang, & Zhang, 2022) aims to achieve high transferability by attacking the relevance map, a common property across interpreters in detectors. *Local Perturbations with Adaptively Global Attacks (LGP)* (G. Li, Xu, Ding, & Xia, 2024) is a detector-agnostic method that works across different models and datasets. LGP focuses perturbations on object regions, avoiding unnecessary changes in background areas. A recent method that exhibits high transfer performance is *Object-Aware Significant Feature Distortion (OSFD)* (Ding et al., 2024). It combines a loss function and a designed data augmentation method that suppresses significant features and amplifies the vicinal features to create false detections that transfer well to other detectors.

2.2.5 Other outputs

Some attacks can be used in several configurations with different outcomes. *Seeing isn't Believing* (Zhao et al., 2019) is composed of two attacks using feature interference reinforcement (FIR) and enhanced realistic constraints generation (ERG) for the vanishing one and nested-AE for the fabrication one. FIR deals with interfering with the internal features of the model to increase robustness, while ERG focuses on making the generated adversarial example more realistic and adaptable to real-world conditions. This approach helps the attack remain effective across different distances. *Targeted Adversarial Objectness Gradient Attacks (TOG)* (Chow et al., 2020) is a suite of adversarial attacks that exploits gradients of the detector loss function to generate different perturbations with different outcomes: random output, object vanishing, object fabrication, and mislabeling.

Adversarial Attacks That Evade Context Consistency Checks (ADC) is a method that generates adversarial images to both deceive object detectors and bypass context consistency checks (Yin et al., 2022). ADC can be deployed as a mislabeling, vanishing, or fabrication attack. Addressing the specific challenge of attacking modern transformer-based detectors, the *Attention-Focused Offensive Gradient (AFOG)* attack (Yahn et al., 2025) uses a learnable attention mechanism to dynamically focus perturbations on vulnerable image regions for random output generation. AFOG also includes specialized modes for vanishing and fabrication.

ShiftAttack (H. Li et al., 2024) has a unique objective where it targets post-processing techniques, such as Non-Maximum Suppression, to generate the adversarial image. It exploits predictions with low intersection over Union in the detectors and boosts their confidences so that they replace the ones with higher IoU, leading to mislocalization and missed detections.

2.3 A review of adversarial defense methods

Countermeasures against adversarial attacks on object detectors can be categorized by the stage at which they intervene: during model training, by modifying the model's architecture or inputs, or by adding external detection modules. These approaches are sometimes adapted from fundamental defense strategies from image classification to the more complex task of object detection.

2.3.1 Adversarial training and training modification

Adversarial training remains the most effective and researched defense strategy. This approach involves augmenting the training set with adversarial examples, thereby making it more adversarially robust.

One of the initial efforts to adapt this technique for object detection proposed generating adversarial examples through the lenses of a multitask learning problem (H. Zhang & Wang, 2019). Adversarial training was further improved through the following contributions. *Class-Aware Robust Adversarial Training (CWAT)* was introduced to solve the class imbalance problem (P.-C. Chen, Kung, & Chen, 2021), which was not taken into account by naive adversarial training,. This method implements a class-wise regularization term to account for class imbalances during training. Other

methods seek to refine the learning process itself. *RobustDet* introduces adversarially-aware convolutions to disentangle feature learning between clean and adversarial images combined with an Adversarial Image Discriminator (AID) (Dong, Wei, & Lin, 2022). However, later research suggests the AID component is primarily effective against strong perturbations and less so for weaker ones (X. Li, Chen, & Hu, 2025). A recent and highly effective approach leverages adversarially pre-trained backbones; for instance, it has been demonstrated that initializing an object detector with a backbone pre-trained on adversarial examples, rather than clean ones, significantly boosts adversarial robustness without altering the detector’s architecture (X. Li et al., 2025).

There also exist instances where adversarial training is used to defend against adversarial patches. For example, *Meta Adversarial Training (MAT)* (Metzen, Finnie, & Hutmacher, 2021) combines adversarial training with a meta-learning framework for universal patches, thereby increasing robustness against universal patch attacks.

There also exist approaches that modify the training process. For example, it has been observed that detectors can be fooled by patches placed outside an object’s bounding box, which exploits the model’s reliance on spatial context (Saha et al., 2020). To mitigate this, the authors proposed limiting the use of spatial context during training, making the detector less dependent on potentially exploitable contextual cues and more robust to such attacks.

2.3.2 Model modification and input transformation

Beyond data augmentation and training process, modifying the model’s intrinsic architecture or adding components that will transform the inputs allows for the creation of robust models that are trained on standard data.

Architecture transformation can make models intrinsically more robust at the cost of often making the model more complex. One such modification involves integrating *Gabor convolutional layers* into the backbone of object detectors (Amirkhani & Karimi, 2022). These filters extract robust spatial features, and by training them as standard network parameters in the first layer, this method enhances resilience to adversarial attacks without degrading performance on benign inputs.

Input transformation acts as a preprocessing step to filter an image before it is fed to the detector. This approach can be model-agnostic. Simple methods like JPEG compression can incidentally degrade adversarial perturbations; however, they are not a complete defense by themselves and must be combined with other methods. More sophisticated techniques employ dedicated models for purification. One such defense utilizes an autoencoder framework coupled with a critic network during training (Zhou, Liu, & Zhou, 2023). In this setup, the critic guides the encoder to map both benign and adversarial inputs to a common, robust feature distribution. The decoder then reconstructs a “clean” version of the image from this robust representation, which is then passed to the object detector.

2.3.3 Adversarial detection

Rather than purifying an image, some defenses focus on detecting whether an input is adversarial or not. These methods act as a gatekeeper, flagging and rejecting suspicious inputs.

The *SCEME* system was proposed as a method to detect adversarial examples by identifying context inconsistencies (S. Li et al., 2020). This approach identifies abnormal statistical relationships between objects and their context that typically arise from adversarial perturbations. *SCEME* learns these context consistency rules during training using a set of class-specific auto-encoders. At inference time, a context profile is extracted for each detected region and fed to the corresponding auto-encoder.

Most adversarial detection methods focus on adversarial patch detection. Early research in this area focused on identifying patches based on their underlying feature representations (Kim, Yu, & Ro, 2022). Another strategy is to explicitly segment the patch and remove it as employed in *Segment and Complete (SAC)* (J. Liu, Levine, Lau, Chellappa, & Feizi, 2022) which trains a patch segmenter with self-adversarial training for pixel-level localization, after which a shape completion algorithm inpaints the removed area. However, its reliance on training with noisy patches limits its effectiveness against more sophisticated, natural-looking patches.

More recent, model-agnostic methods have shown greater promise against realistic patches. *Jedi* (Tarchoun, Ben Khalifa, Mahjoub, Abu-Ghazaleh, & Alouani, 2023) leverages entropy analysis to identify high-entropy regions likely to contain a patch. It refines this localization using an autoencoder to complete these regions. Building on this, *Patch-Agnostic Defense (PAD)* (Jing, Wang, Ren, Dong, & Zou, 2024) operates without any training by leveraging two universal properties of patches: semantic independence from the scene and spatial heterogeneity compared to their immediate surroundings.

2.3.4 Certified defenses

While the previous methods show empirical success, certified defenses provide a formal, mathematical guarantee of robustness against a specific class of attacks within a defined perturbation budget (L_p -norm ball). The first model-agnostic and training-free certified defense for object detection against L_2 -bounded attacks was established by reducing the detection task to a regression problem and applying median smoothing (Chiang et al., 2020).

For the specific threat of patch attacks, *DetectorGuard* (Xiang & Mittal, 2021) employs an "objectness explaining strategy", using a robustly trained image classifier to scan every location in an image and predict the probability of an object's presence, thereby providing a provable security guarantee against patch hiding attacks. A subsequent work, *ObjectSeeker* (Xiang, Valtchanov, Mahloujifar, & Mittal, 2023), neutralizes patches by masking them entirely without prior knowledge of their appearance or location, and includes a certification procedure to formally guarantee robustness.

2.4 Evaluating attack impact and perceptibility

2.4.1 Evaluation metrics

In order to measure the impact of an attack, it is necessary to use appropriate metrics. Unlike classification, object detection involves localizing and classifying multiple objects, leading to a more complex performance evaluation. Furthermore, the diverse objectives of different adversarial attacks often require tailored metrics. This section

presents the most common metrics among the attack and defense methods listed in Sections 2.2 and 2.3 and highlights their applicability and limitations.

mean Average Precision (mAP) & Average Precision (AP): The AP is calculated by averaging the precision-recall curves for an object class. *Precision* quantifies the ratio of true positives out of all detected objects (True positives and False positives), while *Recall* measures the fraction of true positives out of all actual objects in the image(true positives and false negatives). The mAP is simply the mean of the APs for each object class. When computing this metric, a prediction is considered as valid for a ground truth if their Intersection over Union (IoU) is greater than a chosen threshold. Generally, to calculate the map, this threshold is set at 0.5 (Ding et al., 2024; G. Li et al., 2024; H. Zhang et al., 2020). For adversarial attacks, a significant drop in mAP indicates a successful attack, as it reflects a degradation in the detector’s localization and classification performance. mAP is a comprehensive metric for detector performance, however it does not precisely isolate the specific objective of certain adversarial attacks.

Success rate/Fooling ratio/Attack Success rate (ASR): The ratio of successfully attacked images. The “success” of an attack is a subjective matter, often adapted to the type of attack being studied which makes comparison across papers challenging and hinders benchmarking attempts. In practice, the success rate is used more often for vanishing and mislabeling attacks. For example, in EBAD the Fooling rate is the ratio of images in which the victim object was successfully misclassified at IoU greater than 0.3 to the target label (Cai et al., 2023) whereas in ASC, a prediction is considered as correct if it has an IoU above 0.5 and a confidence score above a threshold depending on the detector used (Y. Zhang et al., 2023). In addition, the Attack Success rate from ShiftAttack is very specific. As it measures the proportion of objects not assigned by any true positive prediction box, but also with the existence of a false positive box of the same label having a valid IoU (H. Li et al., 2024).

False Positive rate (FP rate): The ratio of false positive detections to the total number of predictions. This metric is used mainly by object fabrication attacks (Tang et al., 2024; D. Wang et al., 2021), where creating false detections is the main objective.

2.4.2 Evaluation of the magnitude of the perturbations

Attacks intended to remain imperceptible to evade detection need to contain the magnitude of the perturbations they generate. Generally, a threshold is introduced during the optimization of the attack in order to limit the distance between the original image and the perturbed image according to a certain chosen norm. It is also possible to evaluate this distance after the creation of adversarial images using other norms. Here are defined the distances and norms most commonly used in the literature.

L_p Norms: L_p norms are the most commonly used to calculate the distances between the original images and the adversarial images, and often integrated into the

optimization process to constrain the perturbation budget of the attack. Among them we have:

- **L_0 norm:** Measures the number of perturbed pixels. $\|\delta\|_0 = \sum_{i=1}^N \mathbb{I}(\delta_i \neq 0)$ where δ is the perturbation vector and N is the total number of pixels.
- **L_1 norm:** Calculates the sum of the absolute differences between corresponding pixel values. $\|\delta\|_1 = \sum_{i=1}^N |\delta_i|$
- **L_2 norm (Euclidean distance):** Represents the square root of the sum of squared differences between pixel values. It reflects the average intensity of the perturbation. $\|\delta\|_2 = \sqrt{\sum_{i=1}^N \delta_i^2}$
- **L_∞ norm:** Quantifies the maximum absolute difference between any single pixel's value in the original and perturbed images. $\|\delta\|_\infty = \max_i |\delta_i|$

The attacks are mostly optimized for L_∞ or sometimes L_2 (Cai et al., 2023; Cai, Xie, et al., 2022; Shapira et al., 2023).

Peak-to-noise ratio (PSNR): A metric that quantifies the amount of perturbation or noise introduced into an image. A low PSNR corresponds to a highly distorted image, and vice versa. When it is used, the objective is, therefore, to maintain it above a chosen threshold (Y. Li, Bian, & Lyu, 2018; Y. Li, Tian, et al., 2018; H. Zhang et al., 2020).

It is computed according to the following formula:

$$\text{PSNR} = 10 \log_{10} \frac{\text{MAX}^2}{\text{MSE}} \quad (1)$$

where MAX denotes the maximum possible pixel intensity value, and MSE represents the mean squared error between the original and perturbed images.

Structural Similarity Index Measure (SSIM): SSIM is a perception-based measure to estimate similarity between two images. It considers structural dependency, the idea that spatially-close pixels have strong inter-dependencies, and perceptual phenomena, such as luminance and contrast, rather than pixel-wise distances. In the approaches listed in Section 2.2, SSIM is used after the computing of the adversarial images to estimate the magnitude of the perturbation in a way that more closely reflects human perception (Guesmi et al., 2024; H. Li et al., 2024; Nezami et al., 2021). LGP attack also uses Information-Weighted Structural Similarity Index (IW-SSIM), a version of the Structural Similarity Index (SSIM) incorporating an information-theoretic weighting scheme (G. Li et al., 2024).

2.5 Are there fair comparisons between attacks ?

Comparing different attack methods presented in the previous Section 2.2 is almost impossible. This is due to the lack of a shared benchmark and test method, including common metrics, datasets, and detectors, which reflect the impacts of all attack types rightfully. Table 1 presents the most recent and advanced attacks, detailing

their outcomes, specificities, locality, perturbation cost metrics, and test configurations reported in their original articles. Attacks selected for our unified benchmark are explicitly marked with a dagger (\dagger). Table A1 in appendix lists this information for all attacks presented in Section 2.2.

Regarding the **detectors** employed, there is no doubt that the YOLOv3 (Redmon & Farhadi, 2018) and Faster R-CNN (Ren et al., 2015) detectors stand out as the most widely used, representing both one-stage and two-stage detectors. It is important to note that some attacks can only be generated by a single type of detector, such as PhantomSponges, which can only be generated with a YOLO (Shapira et al., 2023) or R-AP (Y. Li, Tian, et al., 2018) that targets the Region Proposal Network, a component that is mostly present in two-stage detectors and absent from YOLOv3. However, even in these cases, it is always possible to test other detectors in a black-box configuration.

For **datasets**, the vast majority of attacks use widely accepted and accessible datasets such as COCO (Lin et al., 2014), VOC2007 or VOC2012 (Everingham, Van Gool, Williams, Winn, & Zisserman, 2010). COCO-person, a subset of COCO dedicated to person detection, is mostly used by patch-based attacks (H. Huang et al., 2023). Nevertheless, attacks do not all use the datasets in the same way. E.g., OSFD takes a sample of only 2000 images from VOC2012 for its tests (Ding et al., 2024). Attacks designed for specialized applications like aerial surveillance rely on domain-specific datasets like DOTA (Xia et al., 2018) as standard benchmarks are inappropriate (Shrestha et al., 2023).

In terms of perceptibility evaluation, the Euclidean norms L_∞ and L_2 are prevalent. However, their application is not always consistent, leading to potential misinterpretations. A key ambiguity lies in the ϵ parameter. In EBAD (Cai et al., 2023), ϵ denotes the strict L_∞ bound of the final adversarial example. In contrast, CAA (Cai, Xie, et al., 2022) treats ϵ merely as a step-wise constraint during optimization, not a total budget. This inconsistency extends to OSFD which, when parameterized with $\epsilon = 5$ shows a resulting perturbation magnitude of $L_\infty = 7$ (Ding et al., 2024). As these examples show, the parameters are not used in the same way at all. Moreover, L_∞ 's relevance as a model for the human eye's sensitivity to perturbations can be largely disputed, and it would be preferable to turn to more perceptual distances (R. Zhang, Isola, Efros, Shechtman, & Wang, 2018), as can be seen in Section 3.

Finally, to evaluate performance, the mAP is an excellent metric that represents well the effectiveness of a detector. It is widely used in the literature (Ding et al., 2024; Guesmi et al., 2024; H. Huang et al., 2023) but it is sometimes not suitable for representing the specific effect of an attack. Some articles therefore use a Success rate (ASR) which, as mentioned in Section 2.4.1, is different for each objective and, therefore, makes direct comparison between articles impossible (Cai et al., 2023; H. Li et al., 2024; Y. Zhang et al., 2023). Thus, it is necessary to use more standardized metrics, which better describe how the detector is affected by the tested attack.

This lack of a shared benchmark (i.e., same datasets and relevant metrics) is hindering progress in the field as fair comparisons between attacks are not possible.

Table 1 Recent adversarial attacks for object detection: Heterogeneity in experimental settings and applicability hinders a fair comparison. * denotes if the code is publicly available. † denotes attacks that we used in our benchmark. Detector families used: Y: YOLO, F: Faster R-CNN, S: SSD, D: DETR, V: VFNet, C: Cascade R-CNN, M: Mask R-CNN, A: ATSS/Anchor-free, R: RetinaNet, G: Grid R-CNN, L: Libra/FoveaBox/FreeAnchor, T: Transformer-based (e.g., Swin, DAB-DETR, Def-DETR). See Table A1 in Appendix A for a more exhaustive list

NAME	OUTCOME	LOCALITY	PERTURBATION COST	METRICS	DETECTOR FAMILY	DATASET USED
AdvART (Guesmi et al., 2024)	Vanishing	Patch	SSIM	mAP, Success rate	Y	INRIA, MPII
LGP (G. Li et al., 2024)*	Random	Entire image	FID, IW-SSIM, PSNR-B	mAP, Number of attacked targets per image, Success rate	F, T, V, C, A	COCO, DOTA-v1.0
OSFD (Ding et al., 2024)* †	Random	Entire image	L_∞	mAP	F, Y, V, M, D, A	VOC2012
Patch-based FP creation (Tang et al., 2024)	Fabrication	Patch	-	Average instances created, Average Precision Decrease, Average Score Created, FP Rate Increase	Y	DOTA-v1.0, RSOD, NWPU VHR-10
ShiftAttack (H. Li et al., 2024)	Other	Entire image	L_2 , SSIM	Success rate	Y, A, L, R, T	COCO, VOC2007, VOC2012
Targeted context attack (C. Sun et al., 2024)	Mislabeling	Entire image	L_∞	Success rate	F, Y, L, T	COCO, VOC2007
ASC (Y. Zhang et al., 2023)	Vanishing	Entire image	L_0	Success rate	S, Y, F, M, T	COCO, Cityscapes, BDD100K
CAA (Cai, Xie, et al., 2022)* †	Mislabeling	Entire image	L_∞	Success rate	F, Y, R, L, D, T	COCO, VOC2007
EBAID (Cai et al., 2023)* †	Mislabeling	Entire image	L_∞	Success rate	F, Y, A, S, G, R, L, T	COCO, VOC2007
Patches against UAV (Shrestha et al., 2023)*	Vanishing	Patch	-	mAP, Success rate	Y	VisDrone-2019
Phantom Sponges (Shapira et al., 2023)* †	Fabrication, Inference latency	Entire image	L_2	Number of created objects, time, recall	Y	BDD100K, MTSD, LISA, VOC INRIA, COCO-person, CCTV-person
T-SEA (H. Huang et al., 2023)*	Vanishing	Patch	-	AP (for person)	F, Y, S	COCO-person, CCTV-person

3 A unified benchmark for adversarial attacks for object detection

3.1 Proposed unified benchmark

To address the issues established in Section 2.5, this section moves beyond a simple survey to propose a unified benchmark. Our goal is to evaluate attacks under identical and controlled conditions. This framework ensures a fair comparison of white-box effectiveness and black-box transferability by standardizing the detectors, the datasets, and the attack settings. Crucially, it also introduces a common set of metrics to evaluate both attack success and the perceptual cost of the perturbations, allowing for a fair side-by-side analysis.

3.1.1 Choice of metrics

It is imperative to provide common metrics that fairly reflect the impacts of each attack, regardless of their outcomes or characteristics. Object detection involves two tasks: localization and classification. Adversarial attacks tend to disrupt either one of these tasks (localization with vanishing attacks, classification with mislabeling attacks) or both (e.g., random and fabrication attacks) (cf. Figure 2). In addition to the standard metric mAP, which is used to estimate the general impact of an attack on object detection performance, we introduce two new complementary metrics reflecting the impact on localization and classification separately: AP_{loc} and CSR defined below. These metrics draw inspiration from error analysis research for object detection (Bolya, Foley, Hays, & Hoffman, 2020; Hoiem, Chodpathumwan, & Dai, 2012) but have never been applied to adversarial attacks.

AP_{loc} : This metric is calculated in the same way as the mAP, except that all object classes are fused as a single class. Therefore, it reflects the localization capacity of the detector, i.e., its ability to detect the presence of an object. Consequently, this metric is particularly sensitive to vanishing attacks and fabrication attacks.

Classification Success Ratio (CSR): This metric evaluates the detector’s classification capability independent of localization failures. Mathematically, this metric is equivalent to the micro-averaged recall of the detector. It measures the ratio of ground-truth objects detected with the correct class to the total number of ground-truth objects. For each ground-truth object, we select the highest-confidence detection that satisfies the localization constraint ($IoU > \text{threshold}$) and verify that the detection class matches the ground-truth class. The CSR can measure misclassification errors not captured by the AP_{loc} where the object is found but labeled wrong. This makes CSR suitable for quantifying the impact of mislabeling attacks. It is computed as:

$$CSR = \frac{\sum_{c=1}^C TP_c}{N_{GT}} \quad (2)$$

where C is the number of classes, TP_c is the number of correctly classified and localized True Positives for class c , and N_{GT} is the total number of ground truth instances across the entire dataset.

Even if the norms L_∞ and L_2 are very widespread, they do not necessarily represent how the human eye will perceive the perturbation applied to the image. Thus, we propose using perceptual metrics, which better model the perceived difference between the original and attacked images, such as SSIM mentioned in Section 2.4.2 or LPIPS (R. Zhang et al., 2018). These metrics are used in the same manner, between the original image and the final adversarial image, to achieve a fair comparison.

Learned Perceptual Image Patch Similarity (LPIPS) Evaluates the perceptual similarity between two images, better aligning with how humans perceive the images. The metric is based on the findings in (R. Zhang et al., 2018) that internal activations of deep networks (e.g., AlexNet, VGG) trained on classification tasks strongly correlate with human perception. It operates by computing the L_2 distance between the deep feature embeddings of two images.

3.1.2 Choice of detectors

To test our benchmark, we use the MMDetection framework, which allows us to easily use a large number of object detectors (K. Chen et al., 2019). We select a **set of detectors** to represent most detector types: YOLOv3 (Redmon & Farhadi, 2018) and Faster R-CNN (Ren et al., 2015) as they are by far the most used detectors of their categories. YOLOX (Ge et al., 2021) serves as a modern YOLO version. FCOS is an anchor-free detector. DETR (Carion et al., 2020) is a standard transformer-based detector. DINO (H. Zhang et al., 2023) represents modern, fully transformer-based architectures. Mask R-CNN (He, Gkioxari, Dollár, & Girshick, 2017) is included as another example of a model with a transformer backbone. The **backbones** used are Darknet-53 for YOLOv3 and ResNet-50 (He, Zhang, Ren, & Sun, 2016) for Faster R-CNN, FCOS and DETR, CSPNet for YOLOX and Swin transformer (Z. Liu et al., 2021) for Mask R-CNN and DINO.

3.1.3 Choice of datasets

All detectors are trained on COCO (Lin et al., 2014) and tested on the VOC2007 test set (Everingham et al., 2010). This is a standard evaluation setup for most attacks, as COCO-trained models are widely available (e.g., in MMDetection), attacks are often evaluated on VOC and the classes in VOC are a compatible subset of the COCO classes.

3.1.4 Choice of attacks

To ensure a fair and rigorous comparison, we focus on digital, non-patch-based attacks. Indeed, first, physical attacks are excluded as they are difficult to reproduce consistently. Their success depends on real-world variables (e.g., printability, lighting, camera angles) that cannot be standardized within a digital benchmark. Second, we exclude patch-based attacks. These attacks are perceptible by design and operate on a "cost"

model (e.g., patch size, shape, or semantic realism) that is completely different from the perturbation measures used by imperceptible attacks. By focusing on digital, non-patch-based attacks, we can use a common set of metrics (like L_∞ , L_2 , and LPIPS) to meaningfully evaluate the attack impact and perceptual cost.

Within this scope, we select the most effective and recent attacks with available code. The only category not represented is the object vanishing one because no recent attack has available code. This gives us the selection: OSFD (Ding et al., 2024) which reported state-of-the-art attack efficiency for random output, EBAD (Cai et al., 2023), an established mislabeling attack (Nguyen et al., 2025) and PhantomSponges (Shapira et al., 2023) for object fabrication. We also include CAA (Cai, Xie, et al., 2022) to study its unique focus of leveraging contextual information.

We initially considered an earlier object detection attack, TOG (Chow et al., 2020) due to its importance in the literature, but decided against including it. The primary reason is that early attacks like TOG exhibit poor transferability even when the target model belongs to the same model family as the source model or with different implementations of the exact same model (cf. Table 2). This is largely due to a different research focus at their time where achieving attack success on a white-box setting was the primary objective and the transferability of the attack only analyzed qualitatively in the original paper.

Table 2 Performance (mAP in %) metric of YOLOv3 attacked by each TOG variant. ML and LL refer to Most Likely (2nd most probable) and Least Likely class selection strategies.

Detectors	Benign	Untargeted	Fabrication	Vanishing	Mislab. (ML)	Mislab. (LL)
YOLOv3 (MMDet)	75.84	59.47	68.15	66.87	70.24	69.68
YOLOv3 (TOG)	78.72	1.88	37.09	17.22	20.53	16.44

We also evaluated the recent AFOG attack (Yahn et al., 2025), which initially seemed promising, as it is one of the few attacks generated directly on a transformer-based detector. However, similar to older attacks like TOG, the original paper does not focus on the transferability of the generated perturbations. The attack procedure involves resizing the input image during preprocessing. As shown in Table 3, while the attack is highly effective on the resized image (13.23% mAP), its effectiveness collapses when the final adversarial image is resized back to the original input dimensions (66.56% mAP). This extreme sensitivity indicates that the generated perturbation is brittle and unlikely to transfer well under different conditions, making it unsuitable for a benchmark focused on practical, transferable robustness. We ultimately excluded AFOG from our main benchmark due to its lack of robustness under minor transformations as it is unsuitable for a benchmark focused on transferability.

3.1.5 Implementation details

For all attacks, we test the default parameter configuration of the original articles. For EBAD and CAA, where the main parameters ϵ_{EBAD} and ϵ_{CAA} influence the L_∞

Table 3 The mAP (%) metric of the AFOG attack (with $L_\infty = 30$) against DETR in white-box. Attack efficiency significantly degrades when the attacked image of the VOC2007 test set are resized back to their original dimensions.

Attack Configuration	mAP (%) on DETR
AFOG DETR ($L_\infty = 30$) - Attacked Image Size	13.23
AFOG DETR ($L_\infty = 30$) - Resized to Original Size	66.56

size of the perturbations, we also run tests for other values. As mentioned in Section 2.5, ϵ_{EBAD} represents the distance between the original image and the adversarial image, while ϵ_{CAA} represents the norm of the perturbation applied to each iteration of the attack (Cai et al., 2023; Cai, Xie, et al., 2022). We refer to both parameters simply as ϵ in the remainder of the paper to denote the attack strength. In addition, the parameter k of OSFD monitors the amplification of object features (Ding et al., 2024), and parameters ϵ_{PS} , λ_1 and λ_2 of PhantomSponges influence the norm L_2 of perturbations, the number of objects transmitted to the NMS, and the minimization of IoUs (Shapira et al., 2023). These parameters are set to their default values in our experiments: $k = 3$, $\epsilon_{PS} = 70$, $\lambda_1 = 1$, $\lambda_2 = 10$. The IoU threshold is set at 0.5 to compute mAP, AP_{loc} and CSR. For the attack time generation, we deactivated all logging, saving and evaluating steps to ensure fair comparison.

3.1.6 Scenarios

We perform tests in white-box and black-box scenarios for YOLOv3, Faster R-CNN and Mask R-CNN. These models are commonly used in the literature and are compatible with the codebases of most selected attacks. For black-box testing, DETR, FCOS, YOLOX, and DINO are used only as target detectors. As PhantomSponges can only be generated on a YOLO detector and has to be trained on a set of images different from the test images, this attack is generated with a YOLOv3 using the VOC2007 trainval set (Shapira et al., 2023).

For CAA, which is ensemble-based, we consider Faster R-CNN and YOLOv3 as surrogate models, so it uses both these models in a white-box setting. A specificity of the ensemble-based method EBAD is that it is query-based. This means that EBAD uses attacks created on the surrogates and then iteratively queries a "victim model" until the refined attack successfully fools the victim model. To refine the attack, the algorithm uses the inference loss of the victim model. Because it requires access to this loss value, EBAD operates in a grey-box setting, where the attacker has partial information about the victim model. To avoid any kind of confusion in our experiments, for attack generation, we use a white-box setting: The victim model queried by EBAD is one of the surrogate models (Faster R-CNN or YOLOv3). In addition, we test the transferability of this generated attack in a black-box setting. Figure 3 summarizes these interactions between source, victim, and target models for each threat model.

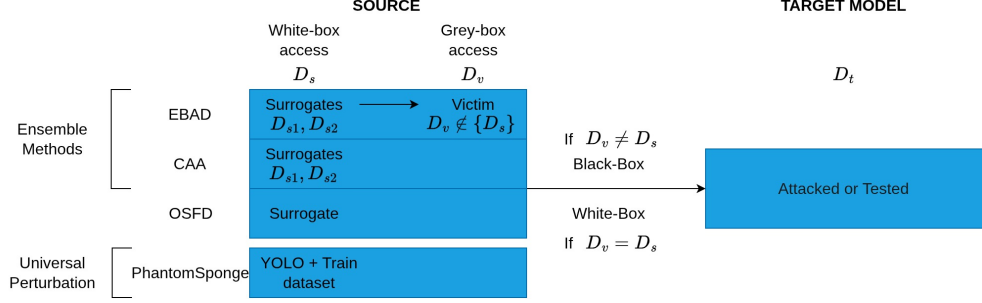


Fig. 3 Threat models for the selected attacks. This diagram illustrates the source models and knowledge access required for generating each attack. D_s denotes the **surrogate models** used for attack generation, while D_v represents the **victim model** queried during the optimization of grey-box attacks (e.g., EBAD). D_t refers to the **target model** used for final evaluation.

3.2 Results and analysis

3.2.1 Quantitative analysis of adversarial perturbation imperceptibility

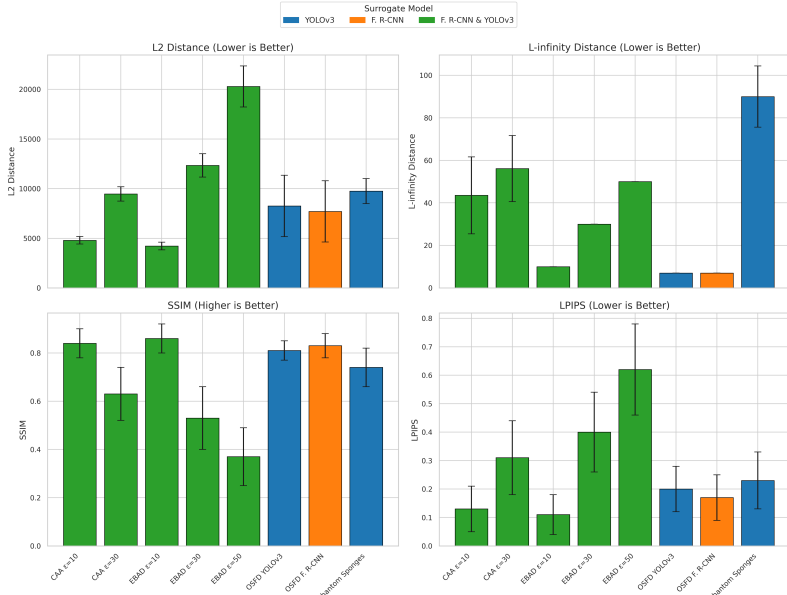


Fig. 4 Quantitative analysis of attack imperceptibility on the VOC2007 test set. The plots illustrate the mean and standard deviation of the perturbations across various distance (L_2 , L_∞) and perceptual (SSIM, LPIPS) metrics.

We now evaluate the imperceptibility of the selected attacks. For each attack, we evaluate each distance or similarity between the original and adversarial images and establish the averages and the standard deviations. Figure 4 plots the mean value and standard deviations for norms L_2 and L_∞ as well as for the perceptual metrics SSIM and LPIPS. The exact values for this plot are available in Table B4 in the appendix. These calculations are performed on non-normalized images, with RGB values between 0 and 255. For OSFD, which resizes images during its attack process, the adversarial images were resized back to their original dimensions before computing L_2 , SSIM, and LPIPS. The L_∞ norm is reported at the attack’s native output resolution to reflect its ϵ -constraint. For the calculation of LPIPS, we used AlexNet as in the original research paper (R. Zhang et al., 2018).

The problem mentioned in Section 2.5 is clearly visualized in Figure 4: The ϵ values of different methods are not comparable, as they are not applied consistently. Although L_∞ is the most commonly used norm in the literature, it completely fails to model the perceptibility of an attack to the human eye. After looking at the different adversarial versions of several images, an example of which is given in Figure 5, the most blatant example is EBAD at $\epsilon = 50$, as while its L_∞ norm of 50 is high, this single number fails to capture the severe visual distortion represented by its LPIPS score of 0.62. An even more compelling case is OSFD (generated on YOLOv3): it has the lowest L_∞ norm in our benchmark (7.0), yet its LPIPS score (0.19) is nearly double that of EBAD at $\epsilon = 10$ (LPIPS 0.11). Based on L_∞ alone, OSFD would be considered the most imperceptible attack, which is visually false (cf. Figure 5(h)). The original work on the LPIPS metric demonstrated that metrics based on deep features align significantly better with human perceptual judgments than traditional metrics (R. Zhang et al., 2018). Supported by this finding we conclude that the LPIPS distance is the most appropriate metric for modeling the perceptibility of adversarial perturbations.

When comparing the LPIPS values to the traditional norms, we observe that the L_2 distance is more strongly correlated with LPIPS than the L_∞ distance. Attacks with lower L_2 values consistently yield lower LPIPS scores, indicating greater imperceptibility. Conversely, attacks with higher L_2 values (EBAD $\epsilon = 50$, CAA $\epsilon = 30$) result in significantly higher LPIPS scores (0.31-0.62). This suggests that L_2 could be a more appropriate constraint for adversarial attacks to align the mathematical perturbation magnitude with human perceptibility.

We also notice across all attacks in Figure 4 the high standard deviation in LPIPS values. For example, CAA ($\epsilon = 30$) shows a mean LPIPS of 0.31 with a standard deviation of 0.13, while the EBAD ($\epsilon = 50$) variant shows standard deviations around 0.14-0.16. This significant variance indicates that the perceptibility of the generated perturbations is not uniform across all images within the dataset for a given attack. This highlights the limitation of evaluating perceptibility metrics across whole datasets and that perceptibility should be evaluated at the image level.

Our empirical findings suggest a strong correlation between LPIPS score and human perception. For instance, attacks with an average LPIPS distance under 0.2 are hardly perceptible to the naked eye whereas attacks with an LPIPS distance above 0.3 have visible artifacts. This observation is purely empirical and finding what level of LPIPS score corresponds to visible alterations for an adversarial attack would require

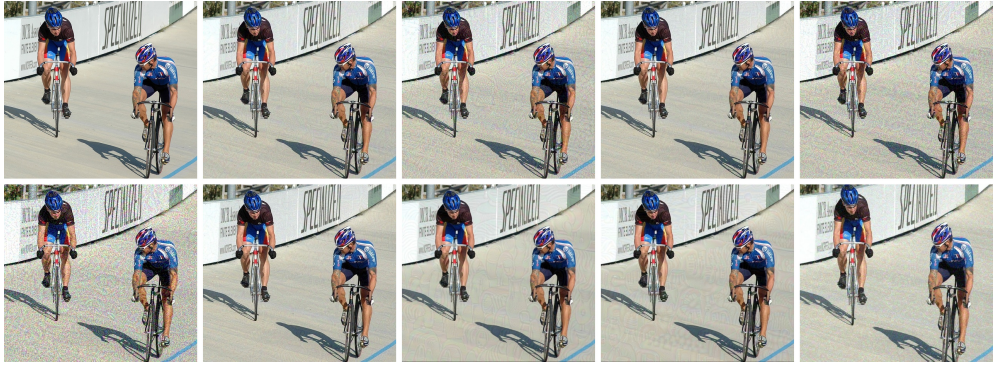


Fig. 5 Visual samples from VOC2007 test set and their perturbed versions. Top row (left to right): benign image, CAA ($\epsilon = 10, 30$), and EBAD on YOLOv3 ($\epsilon = 10, 30$). Bottom row (left to right): EBAD on YOLOv3 ($\epsilon = 50$), EBAD on Faster R-CNN ($\epsilon = 10$), OSFD on YOLOv3 and Faster R-CNN ($\epsilon = 5$), and PhantomSponges ($\epsilon = 70$). Perturbations best viewed with zoom at 300%.

an in-depth study and is beyond the scope of this paper. At an LPIPS of 0.6, images generated with the EBAD ($\epsilon = 50$) variant are significantly distorted, we focus on variants of lower ϵ for EBAD in the following experiments. This is also reflected in the SSIM metric, which shows a clear inverse correlation with LPIPS (e.g., EBAD ($\epsilon = 50$) has both the highest LPIPS and lowest SSIM), suggesting both are effective at identifying severe distortions.

3.2.2 Evaluation of the attacks' impact on detector performance

Tables 5 and 4 show, respectively, the mAP, AP_{loc} and CSR values of the detectors under adversarial attack. We can derive the impact of each attack, with regard to their different outcomes and their black-box transferability across all detectors.

Type of impact:

As we expect, the two mislabeling attacks, CAA and EBAD, particularly affect CSR. Because CAA can sometimes cause the appearance of spurious detections by modifying the context of the images, its impact on localization is greater than EBAD (Cai, Xie, et al., 2022). On the other hand, EBAD focuses solely on mislabeling and therefore has less impact on localization than most other attacks (Cai et al., 2023); for instance, on YOLOv3, EBAD (YOLO) causes a 51.0% drop in CSR compared to only 19.5% in AP_{loc} (cf. Table 4). The OSFD attack, being the newest, is the most effective of the selected attacks in terms of mAP. As an attack with random output, it targets both localization and classification. This is reflected in the AP_{loc} and CSR results which are impressive, especially for AP_{loc} (drop of more than 90% for every model except DINO for OSFD (YOLO)). PhantomSponges is a universal attack and, as expected, is therefore less effective than the others. As the objective of PhantomSponges is to generate new non-existent objects while preserving the original detections, its effect is deliberately very weak on CSR and is less severe than the others on AP_{loc} ($\sim 10\text{-}11\%$ drop) (Shapira et al., 2023).

Table 4 Impact of the selected attacks on detectors’ localization (Relative drop in % compared to the benign AP_{loc} in %) and classification (Relative drop in % compared to the benign CSR in %) abilities. The “Benign” column refers to the absence of attacks. FRC is short for Faster R-CNN. MRC is short for Mask R-CNN

DETECTOR	Backbone	Relative drop in % compared to the benign AP _{loc} / CSR (%)↓							
		Benign		CAA (YOLO,FRC)		EBAD (ε = 30)		OSFD (k = 3)	
		AP _{loc} CSR(%)	ε = 30	YOLO	FRC	YOLO	FRC	YOLO	MRC
YOLOv3	DarkNet-53	79.6 / 85.8	52.1 / 67.8	19.5 / 51.0	18.1 / 40.7	93.5 / 70.2	<u>70.0</u> / 42.8	60.2 / 55.9	10.1 / 11.4
FCOS	ResNet-50	81.6 / 91.3	24.9 / 24.1	16.8 / 29.2	16.8 / 22.8	<u>95.8</u> / <u>69.1</u>	97.9 / 75.9	87.1 / 61.3	11.8 / 9.3
FRC	ResNet-50	82.7 / 89.8	59.7 / 80.7	21.3 / 52.9	20.1 / 43.0	<u>95.2</u> / 66.0	97.5 / <u>72.9</u>	91.5 / 65.9	11.4 / 10.0
DETR	ResNet-50	83.0 / 91.9	35.2 / 28.7	20.1 / 34.3	18.4 / 27.9	<u>93.9</u> / <u>66.7</u>	95.9 / 68.8	92.0 / 66.4	12.5 / 8.3
MRC	Swin-T	81.6 / 91.3	24.9 / 24.1	16.8 / 29.2	16.8 / 22.8	<u>95.8</u> / <u>69.1</u>	97.9 / 75.9	87.1 / 61.3	11.8 / 9.3
YOLOX-1	CSPNet	89.5 / 94.2	7.7 / 7.5	8.4 / 10.7	7.4 / 8.8	89.3 / 63.4	74.3 / 43.0	<u>76.3</u> / <u>55.4</u>	13.7 / 11.1
DINO	Swin-L	89.9 / 96.9	2.8 / 2.3	3.6 / 2.8	3.6 / 2.3	<u>29.9</u> / <u>12.4</u>	16.9 / 5.2	43.4 / 18.5	1.7 / 0.9

Table 5 Impact of the selected attacks on detectors’ performance (Relative drop in % compared to the benign mAP in %). The “Benign” column refers to the absence of attacks. The final row shows the average attack generation time per image on a NVIDIA TITAN RTX. FRC is short for Faster R-CNN. MRC is short for Mask R-CNN

DETECTOR	Backbone	Benign mAP	Relative drop in % compared to the benign mAP ↓							
			CAA (YOLO,FRC)		EBAD ($\epsilon = 30$)		OSFD ($k = 3$)		Phantom Sponges	
			$\epsilon = 10$	$\epsilon = 30$	YOLO	FRC	YOLO	FRC	MRC	
YOLOv3	DarkNet-53	75.8	83.8	92.1	74.5	69.3	<u>91.3</u>	70.4	67.3	16.0
FCOS	ResNet-50	78.9	17.7	41.2	39.0	36.0	<u>92.6</u>	96.7	88.7	18.8
FRC	ResNet-50	79.3	89.0	95.7	72.5	67.1	<u>90.7</u>	95.7	89.8	17.2
DETR	ResNet-50	80.3	23.9	54.7	53.9	47.4	89.5	93.4	<u>89.8</u>	18.4
MRC	Swin-T	86.9	5.6	15.8	17.1	16.7	<u>85.5</u>	77.6	99.4	10.9
YOLOX-l	CSPNet	87.5	3.8	10.6	12.1	10.9	<u>84.3</u>	70.2	76.1	19.1
DINO	Swin-L	89.6	0.7	3.8	4.5	4.4	<u>27.3</u>	15.4	40.2	2.3
Time per image (s)		-	84 s		17 s		44 s		N/A (Universal)	

Transferability:

The most effective attack on a large number of detectors is OSFD, which is also the most recent and based on feature manipulation. This is a random output attack that achieves high transferability while remaining highly effective on all detectors tested in white-box and black-box configurations causing mAP drops exceeding 84% on all CNN-based models (Table 5). It is worth noting that this efficiency comes at a significant computational cost. As shown in the final row of Table 5, OSFD requires an average of 44 seconds per image in our benchmark, making it considerably slower than the highly-efficient EBAD (17 s) but faster than the context-aware CAA (84 s). For the other attacks, we remark that CAA is more efficient in a white-box setting (e.g., 95.7% drop on FRC vs 67.1% drop on FRC for EBAD) compared to EBAD that exhibits more transferability in a black-box setting (e.g., 12.1% drop on YOLOX vs 10.6% for CAA).

In terms of **detectors**, the most recent models such as YOLOX (Ge et al., 2021) or DINO (H. Zhang et al., 2023) exhibit better robustness. This can partially be attributed to the fact that they are always tested in black-box configuration and without ever being part of the surrogate models EBAD, CAA and OSFD. For EBAD and OSFD, it is the attacks generated on YOLOv3 that achieve better transferability across detectors except for DINO. Another interesting finding is the existence of a significant gap in transferability between **architectures**, particularly from Convolutional Neural Networks (CNNs) to Vision Transformers. We can also note the robustness of DINO, which consistently maintains high performance against attacks transferred from other models, restricting the mAP drop to 27.3% for OSFD and under 5% for other attacks

(Table 5). As there are currently no attacks in our benchmark capable of compromising modern detectors in a realistic black-box scenario, future research must focus on formulating new black-box attacks designed to challenge these modern architectures.

4 How to defend object detectors against the most efficient attacks?

4.1 Performing adversarial training

Although the field of adversarial attacks has progressed a lot in recent years, the same cannot be said for defense methods, which are much less numerous, as shown in Section 2.3. To our knowledge, adversarial training is currently the defense method with the greatest potential to make detectors robust against the largest number of attacks at once (Amirkhani & Karimi, 2022). A key objective of this work is to systematically evaluate which attacks are most suitable for generating effective training data. In order to make the best use of this method, we fine-tune our detectors using images perturbed by state-of-the-art attacks. We are also mixing adversarial images from different attacks in the adversarial training dataset, hoping to observe a positive effect and thus making the detector even more robust. The goal is to identify effective adversarial training strategies (which attacks/combinations) to maximize detector robustness while maintaining performance on benign images.

For this experiment, we select the same attacks as in Section 3. The adversarial examples are generated in a white-box configuration on the tested detector (Faster R-CNN or YOLOv3) as this ensures the attack is specifically tailored to the model we are defending and represents its "worst-case" scenario. There are two exceptions: CAA does not consider a victim model (Cai, Xie, et al., 2022), and PhantomSponges, which is always generated with a YOLOv3 (Shapira et al., 2023), as explained in Section 3.1.4.

We include attack configurations that may lead to more perceptible perturbations (as discussed in Section 3) because such stronger adversarial examples are valuable for potentially inducing greater robustness during the adversarial training process.

Comprehensive data is provided in the Appendix, including the full comparison for both YOLOv3 and Faster R-CNN (Tables C5 and D6) as well as the detailed metric breakdowns (mAP, AP_{loc}, and CSR) for the Faster R-CNN experiments (Tables D7, D8, and D9).

4.2 Experimental setup

In this section, we use Faster R-CNN (Ren et al., 2015) and YOLOv3 (Redmon & Farhadi, 2018) introduced in Section 3.1.2. To perform the adversarial training, we still use the MMDetection framework (K. Chen et al., 2019). Each adversarial training process is performed in the same way. As explained, the two detectors were pre-trained on COCO (Lin et al., 2014) and are now being fine-tuned on the adversarially attacked VOC2007 trainval set (Everingham et al., 2010). The learning rate is always set to 0.0001 and the number of epochs is set to 50 for YOLOv3 and 20 for Faster R-CNN. As in Section 3, the test dataset is VOC2007 test set (Everingham et al., 2010). We still

use the IoU threshold of 0.5 for mAP, AP_{loc} and CSR. When using a mixed adversarial training dataset, the images altered by the different attacks come from original images that are always different; there are never two adversarial versions of the same image in a single adversarial training set ensuring that the training set benefits from a wider diversity of images.

4.3 Evaluation of the robustness of detectors after adversarial training

We fine-tune each detector using adversarial images of several attacks and then we test them against the same set of attacks as in Section 3. For comparison, we also test the "Baseline" detector, i.e., without adversarial training, and the "Benign" detector, i.e. fine-tuned on unattacked images. For each attack, the same metrics show its impacts on defended models, as discussed in Section 3.

4.3.1 Comparison of the impact of each attack on defense by adversarial training

We observe (cf. Tables 6 and 7) that even fine-tuning on benign images almost always improves the robustness of the detectors, particularly against mislabeling attacks (e.g., mAP against EBAD $\epsilon = 10$ improves from 22.0% to 48.7%). Given that our detectors are trained on COCO and then fine-tuned and tested on subsets of VOC2007, we can conclude that the reduction of the domain gap for the test makes the detector more robust against this type of perturbation. Indeed, this effect is more noticeable with mAP and CSR than with AP_{loc} .

Table 6 also clearly illustrates the expected robustness-accuracy trade-off: For adversarial training made on EBAD, the more the magnitude of the perturbations increases, the more the performance on adversarial images increases (e.g., against CAA $\epsilon = 30$, mAP rises from 38.1% to 66.8%) at the expense of performance on original images (benign mAP drops from 75.4% to 68.7%). This confirms that achieving broad robustness requires accepting a compromise in benign performance.

Do specific attacks provide superior robustness? OSFD and CAA lead to the most robust detectors overall. This points to a critical result: the robustness gained from training on one attack does not necessarily generalize to all others. Specifically, robustness does not transfer well from weaker to stronger attacks. This is most evident when testing against OSFD: Models trained on CAA $\epsilon = 30$ or EBAD $\epsilon = 50$ are still vulnerable to OSFD (mAP of 53.0% and 49.4%, respectively). However, the reverse is not true: the OSFD-trained model performs well against CAA and EBAD (mAP $\geq 65\%$ against both).

Similarly, using a universal perturbation such as PhantomSponges for adversarial training leads to weaker improvement as expected from a unique perturbation.

4.3.2 Adversarial training on partially attacked datasets

To find an optimal accuracy-robustness trade-off, this experiment investigates if an equilibrium can be found by performing adversarial training on datasets containing only a proportion of adversarial images mixed with benign ones. We fine-tune YOLOv3

Table 6 Performance (**mAP** in %) of **YOLOv3** detectors defended by adversarial training. The subscript next to CAA and EBAD indicates their respective ϵ parameters. For EBAD attacks, the target model is YOLOv3. For OSFD and Phantom Sponges, the model mentioned is the surrogate used for attack generation. Higher is better.

FINE-TUNED ON	Benign	CAA ₁₀	CAA ₃₀	EBAD ₁₀	EBAD ₃₀	OSFD	OSFD	Phantom Sponges
						YOLOv3	F. R-CNN	YOLOv3
Baseline	75.8	12.3	6.0	22.0	19.3	18.1	6.6	22.4
Benign	75.8	28.0	17.1	48.7	32.7	28.1	8.3	23.3
CAA ₃₀	72.2	<u>72.2</u>	<u>66.3</u>	<u>72.1</u>	<u>67.4</u>	<u>60.6</u>	<u>53.0</u>	<u>61.6</u>
EBAD ₁₀	<u>75.4</u>	67.0	38.1	70.1	51.8	39.3	36.9	53.2
EBAD ₅₀	68.7	69.4	66.8	70.0	68.8	66.0	49.4	57.7
OSFD	73.5	73.9	65.1	73.6	65.2	53.5	69.1	69.8
Phantom Sponges	74.1	62.6	35.4	67.6	48.0	36.2	27.3	45.2
								73.0

Table 7 Localization (AP_{loc} in %) and classification performance (CSR in %) of **YOLOv3** detectors defended by adversarial training. The subscript next to CAA and EBAD indicates their respective ϵ parameters. For EBAD attacks, the target model is YOLOv3. For OSFD and Phantom Sponges, the model mentioned is the surrogate used for attack generation. Higher is better.

FINE-TUNED ON	Benign	CAA ₁₀	CAA ₃₀	EBAD ₁₀	EBAD ₃₀	EBAD ₅₀	OSFD	OSFD YOLOv3	F. R-CNN	Phantom Sponges	YOLOv3
Baseline	79.6 / 85.8	41.6 / 37.6	38.1 / 27.6	64.7 / 42.1	64.1 / 42.0	64.0 / 41.7	5.2 / 25.6	23.9 / 49.1	71.6 / 76.0		
Benign	80.0 / 83.8	49.7 / 50.4	42.9 / 42.9	65.6 / 60.9	63.5 / 49.7	62.9 / 46.2	5.2 / 22.3	24.1 / 43.3	70.2 / 72.3		
CAA ₃₀	77.5 / 82.1	<u>77.1 / 80.5</u>	73.7 / 75.0	<u>76.5 / 79.4</u>	<u>72.9 / 74.5</u>	<u>69.4 / 68.4</u>	<u>60.0 / 68.2</u>	<u>68.2 / 74.4</u>	<u>72.7 / 77.4</u>		
EBAD ₁₀	79.6 / 84.4	73.8 / 76.2	57.2 / 59.4	74.8 / 76.9	67.6 / 63.1	65.2 / 54.6	39.8 / 59.6	58.7 / 71.0	72.6 / 76.5		
EBAD ₅₀	74.5 / 79.9	74.9 / 79.4	73.4 / 76.7	75.1 / 78.5	74.1 / 76.5	72.8 / 73.9	57.5 / 66.4	65.2 / 72.6	71.1 / 77.1		
OSFD	77.7 / 82.2	77.7 / 81.3	72.3 / 73.0	77.3 / 80.5	71.6 / 72.0	66.6 / 62.7	73.8 / 78.1	74.6 / 79.3	70.9 / 74.5		
Phantom Sponges	78.7 / 83.3	71.1 / 73.1	55.1 / 56.7	73.7 / 75.0	66.7 / 60.7	64.5 / 52.3	33.7 / 49.0	52.2 / 64.2	77.0 / 81.2		

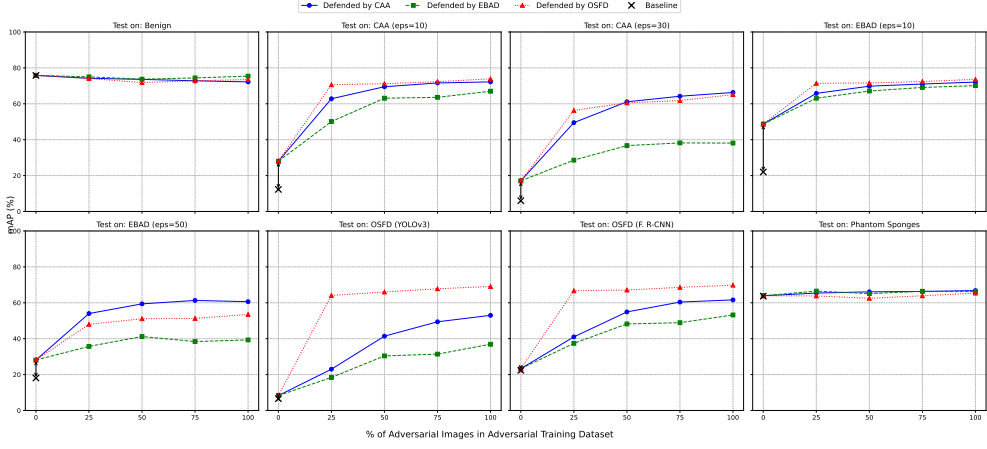


Fig. 6 Performance (mAP in %) of YOLOv3 fine-tuned with varying percentages of adversarial images produced by three different attacks (CAA₃₀, EBAD₁₀ and OSFD (YOLO)) and tested across eight different adversarial attacks.

on training sets composed of 25%, 50%, and 75% adversarial images (generated by CAA $\epsilon = 30$, EBAD $\epsilon = 10$ and OSFD (YOLO)), with the remainder of the dataset being benign images. We then evaluate these fine-tuned models against models trained on 100% adversarial images.

The observed results in Figure 6 show that the performance gain on unattacked images is often low compared to the performance drop on adversarial images. For example, the OSFD-trained model's performance only degrades from 75.8% mAP (at 0% adversarial) to 73.5% mAP (at 100% adversarial). This minor 2.3 percentage point (p.p.) loss in benign accuracy is dramatically outweighed by the massive gain in robustness across all attacks. This trade-off is particularly poor at 25% of attacked images in the adversarial training dataset. For example, the robustness of the CAA-trained model against OSFD (YOLO) plummets from 53.0% mAP (at 100% adversarial) to just 23.0% mAP (at 25% adversarial) for a recovery of 2% mAP on the benign dataset. These results suggest that conducting adversarial training with a fully attacked dataset is likely the more efficient strategy.

Our results show that while OSFD provides the best general robustness, it still leaves the model vulnerable to high-magnitude attacks like EBAD $\epsilon = 50$. Similarly, EBAD $\epsilon = 50$ training confers strong robustness against mislabeling but fails to protect against OSFD. This suggests that mixing attacks with different outcomes (random output for OSFD and mislabeling for EBAD) could cover these complementary weaknesses.

4.3.3 Adversarial training on mixed-attack datasets

We first test mixing the two best-performing single attacks, OSFD and CAA $\epsilon = 30$ (Tables 8 and 9) in different proportions. The results show a minor benefit: the OSFD 75% CAA₃₀ 25% mix achieves a slightly better mAP against EBAD $\epsilon = 50$

Table 8 Performance (mAP in %) of **YOLOv3** detectors defended by adversarial training with various mixed dataset compositions. The subscript next to CAA and EBAD indicates their respective ϵ parameters. For EBAD attacks, the target model is YOLOv3. For OSFD and Phantom Sponges, the model mentioned is the surrogate used for attack generation. Bold and underlined are respectively best and second best YOLO defended models. Higher is better.

	FINE-TUNED ON	Benign	CAA $\epsilon = 10$	CAA $\epsilon = 30$	EBAD $\epsilon = 10$	EBAD $\epsilon = 30$	YOLOv3	YOLOv3	YOLOv3	YOLOv3	F. R-CNN	OSFD	OSFD	Phantom Sponges	YOLOv3
Benign		75.8	28.0	17.1	48.7	32.7	28.1		8.3	23.3		63.9			
CAA ₃₀		72.2	72.2	66.3	72.1	67.4	60.6		53.0	61.6		66.8			
OSFD		<u>73.5</u>	73.9	65.1	73.6	65.2	53.5		69.1	69.8		65.4			
EBAD ₅₀		68.7	69.4	66.8	70.0	68.8	<u>66.0</u>		49.4	57.7		64.7			
OSFD 50% CAA ₃₀ 50%		72.2	72.9	67.6	72.8	67.6	59.5		67.2	68.5		66.8			
OSFD 75% CAA ₃₀ 25%		73.1	73.5	67.5	73.6	67.6	58.4		68.2	<u>69.3</u>		67.4			
OSFD 33% CAA ₃₀ 33%		71.7	72.1	65.6	71.8	67.0	59.0		65.9	67.4		66.0			
Benign 34%															
OSFD 50% EBAD ₅₀ 50%		71.9	72.6	<u>69.5</u>	73.0	69.7	65.2		67.2	68.7		<u>67.1</u>			
OSFD 25% EBAD ₅₀ 75%		70.8	71.8	<u>69.5</u>	71.9	<u>69.9</u>	66.2		65.5	67.0		65.7			
OSFD 75% EBAD ₅₀ 25%		73.0	<u>73.7</u>	69.6	<u>73.5</u>	70.0	64.8		<u>68.9</u>	69.8		67.4			

Table 9 Localization (AP_{loc} in %) and classification performance (CSR in %) of **YOLOv3** detectors defended by adversarial training with various mixed dataset compositions. The subscript next to CAA and EBAD indicates their respective ϵ parameters. For EBAD attacks, the target model is YOLOv3. For OSFD and Phantom Sponges, the model mentioned is the surrogate used for attack generation. Bold and underlined are respectively best and second best YOLO defended models. Higher is better.

FINE-TUNED ON		Benign	CAA $\epsilon = 10$	CAA $\epsilon = 30$	EBAD $\epsilon = 10$	EBAD $\epsilon = 30$	YOLOv3	YOLOv3	EBAD $\epsilon = 50$	OSFD	OSFD	Phantom Sponges
									YOLOv3	F. R-CNN	YOLOv3	
Benign		80.0/83.8	49.7/50.4	42.9/42.9	65.6/60.9	63.5/49.7	62.9/46.2	5.2/22.3	24.1/43.3	70.2/72.3		
CAA ₃₀		77.5/82.1	77.1/80.5	73.7/75.0	76.5/79.4	72.9/74.5	69.4/68.4	60.0/68.2	68.2/74.4	72.7/77.4		
OSFD		<u>77.7/82.2</u>	77.7/81.3	72.3/73.0	<u>77.3/80.5</u>	71.6/72.0	66.6/62.7	73.8/78.1	74.6/79.3	70.9/74.5		
EBAD ₅₀		74.5/79.9	74.9/79.4	73.4/76.7	75.1/78.5	74.1/76.5	<u>72.8/73.9</u>	57.5/66.4	65.2/72.6	71.1/77.1		
OSFD 50% CAA ₃₀ 50%		76.8/81.6	77.4/81.4	73.9/76.1	77.0/80.3	73.2/74.8	69.4/68.3	72.4/76.8	73.3/77.9	72.7/76.9		
OSFD 75% CAA ₃₀ 25%		77.3/81.2	<u>77.6/81.2</u>	74.2/75.4	77.4/80.3	73.0/74.0	69.1/66.8	73.0/77.1	73.9/78.2	72.4/76.7		
OSFD 33% CAA ₃₀ 33%		76.3/79.4	76.5/79.1	72.9/73.5	76.2/78.2	72.5/73.4	69.4/67.8	71.3/74.8	72.6/75.8	71.8/74.9		
Benign 34%												
OSFD 50% EBAD ₅₀ 50%		76.7/81.5	<u>77.2/81.3</u>	75.5/77.8	77.2/ 80.6	<u>74.7/77.1</u>	72.5/73.7	72.6/77.3	73.6/78.5	<u>72.6/77.8</u>		
OSFD 25% EBAD ₅₀ 75%		77.2/81.9	77.7/81.3	<u>75.1/77.5</u>	<u>77.3/80.6</u>	<u>74.7/76.7</u>	72.0/72.6	<u>73.3/77.8</u>	<u>74.2/78.7</u>	72.7/77.5		
OSFD 75% EBAD ₅₀ 25%		75.8/80.5	76.7/80.7	75.4/78.3	76.6/79.7	75.1/77.2	73.1/74.2	71.4/75.9	72.5/77.1	72.1/76.7		

(58.4%) than OSFD alone (53.5%). Next, we test mixing OSFD with EBAD $\epsilon = 50$. The results show a clear synergistic effect. The OSFD 75% EBAD₅₀ 25% model, for instance, produces a detector that is superior to the OSFD-only model. While it retains the robustness of OSFD (e.g., 68.9% mAP vs. OSFD (YOLO)), it achieves 64.8% mAP against EBAD $\epsilon = 50$, a massive improvement over the 53.5% mAP from the OSFD-only model. We also tested adding 34% of unattacked images to this mix, but it does not provide many clear benefits.

These mixtures demonstrate the positive effect that can be obtained for adversarial training by using attacks with different outcomes, especially if these outcomes are very different, such as with random output (OSFD) and object mislabeling (EBAD) used here. This indicates that the training forces the model to learn more robust features against spatial (localization) and semantic (classification) perturbations.

5 Future directions

5.1 Bridging the Cross-Architecture Transferability Attack Gap

There is a notable gap in the literature regarding adversarial attacks generated on newer or different detectors. This includes more up-to-date versions of YOLO or end-to-end transformer architectures such as DINO. So far, few attacks have used the latter to generate their perturbations (Cai et al., 2023) (cf. Section 3). This is largely because most existing attack codebases rely on older frameworks (e.g., earlier versions of MMDetection for EBAD, CAA and OSFD) that do not include these modern detectors. Furthermore, even recent attacks that do include these modern detectors, such as AFOG (Yahn et al., 2025), often do not focus on cross-architecture transferability, which highlights a blind spot in current attack methodologies.

Beyond targeting the output of detectors, attacks that focus on high-level representations to generate perturbations like OSFD (Ding et al., 2024) yield promising results. Feature-based attacks could be explored as a way of formulating attacks with better cross-architecture transferability (Ding et al., 2024) (cf. Section 3).

A special focus should be made around the transferability of black-box attacks for modern detectors. Our findings show that attacks seem to be less transferable for modern detectors, especially cross-architecture. Just as we have done in our benchmark, we hope that future attack methodologies will be consistently evaluated in a black-box scenario against a panel of modern detectors to better assess their transferability.

5.2 Adversarial training and new defense strategies

There are still various aspects of adversarial training that need to be explored. While this work focused on cross-detector transferability, a critical open question remains regarding cross-dataset transferability. In real-world deployment, the attack environment often differs significantly from the training domain (e.g., different weather conditions, lighting, or sensor types) (Khodabandeh, Vahdat, Ranjbar, & Macready, 2019). It remains unclear how well adversarial training on a standard benchmark generalizes to these out-of-distribution scenarios. A significant open question in the

literature is whether the robustness gained from adversarial training is domain-specific or if it can help bridge the domain gap between disparate environments (Fujii, Kera, & Kawamoto, 2022).

Research is also needed for new defense methods (cf. Section 2.3). At the moment, the number of methods is rather limited, but progress could be made. Drawing inspiration from classification, important improvements could be made with methods such as Adversarial purification (Nie et al., 2022), which attempts to remove perturbations before the image is fed to the model with the use of generative models. Another possibility would be to improve adversarial training by including other methods such as Tradeoff-inspired Adversarial Defense via Surrogate-loss minimization (TRADES), which focuses on the fact that improving robustness against adversarial attacks often comes at the cost of accuracy. They focus on optimizing the original error while minimizing the distance between predictions of original and adversarial examples (H. Zhang et al., 2019).

5.3 Standard framework for patch-based attacks

Our observations about the lack of standard evaluation for attacks for object detection can be extended to patch-based attacks (H. Huang et al., 2021; Y. Li, Bian, & Lyu, 2018) and physical attacks (Xu et al., 2020; D.Y. Yang et al., 2018) even though the literature about patch-based attacks for object detection is quite developed. A key question is how can we design a standard benchmark and metrics for this distinct threat model? For example, for patch-based attacks, the perceptibility of a patch is related to factors like patch size or the semantic consistency with its environment which are measured differently than standard L_p distances. Similarly, physical attacks and adversarial objects must remain effective even when subjected to a wide range of natural transformations that do not exist in the purely digital domain, such as changing lighting conditions, different viewing angles, and partial occlusions, etc.

6 Conclusion

In this paper, we addressed the critical lack of standardized evaluation in adversarial attack and defense of object detectors. We provided a review of adversarial attacks and defenses in object detection that identified the disparate datasets, inconsistent metrics, and non-comparable perturbation measures, making fair comparisons impossible. To resolve this fragmentation, we proposed a unified benchmark framework focusing on digital, non-patch-based attacks. By enforcing consistent datasets, metrics, and perturbation constraints, our framework enables the first direct comparison of these methods. This benchmark introduces specialized metrics (AP_{loc} and CSR) to disentangle localization and classification errors and leverages perceptual metrics (LPIPS, L_2) to provide a fair measure of attack cost or perceptibility.

Using this benchmark, our comparison of SOTA attack performance led to several key findings. We identified OSFD as the most effective and broadly transferable attack, but highlighted its significant computational cost (44s per image). Our analysis also reveals the crucial compromises with perceptibility, demonstrating that the L_∞ norm is a poor proxy for human perception and that perceptual metrics like LPIPS are

essential for fair comparisons. Critically, we found that black-box transferability is not uniform: attacks generated on YOLOv3 (like EBAD and OSFD) transfer well to other CNNs, but we revealed a significant cross-architectural robustness gap, as all tested attacks fail to transfer to modern transformer-based architectures like DINO. On the defense side, our experiments on adversarial training identified clear strategies. We demonstrated that using a 100% adversarially-attacked dataset is superior to mixing with benign images, as the minimal loss in benign accuracy is a worthwhile trade-off for the substantial gain in robustness. Most importantly, we found that the strongest defense is achieved by training on a mix of high-perturbation, complementary attacks (e.g., spatial and semantic), which successfully covers the weaknesses of any single, strong attack and achieves the highest overall robustness.

Our work provides this clear comparison of modern attacks and defenses, establishing best practices for adversarial defense and identifying the cross-architecture robustness of transformers as the next major frontier for both attackers and defenders.

Declarations

Author information

- Alexis Winter: <https://orcid.org/0009-0000-3006-525X>
- Romaric Audigier: <https://orcid.org/0000-0002-4757-2052>
- Angelique Loesch: <https://orcid.org/0000-0001-5427-3010>
- Bertrand Luvison: <https://orcid.org/0000-0003-2475-3712>

Funding

Funded by the European Union. Views and opinions expressed are however those of the author(s) only and do not necessarily reflect those of the European Union nor the European Commission. Neither the European Union nor the granting authority can be held responsible for them. This work was supported under the EDF Project FaRADAI (grant number 101103386). This work was made possible by the FactoryIA supercomputer (funded by the Ile-de-France Regional Council). This work was supported by a State grant managed by the French National Research Agency, Agence Nationale de la Recherche, under "France 2030" (grant reference "ANR-22-PECY-0011", within the framework of the "COMPROMIS" project).

Competing interests

The authors have no relevant financial or non-financial interests to disclose.

Data availability

The PASCAL VOC 2007 dataset (Everingham et al., 2010) used during the current study is available in the official PASCAL VOC repository: <https://www.robots.ox.ac.uk/~vgg/projects/pascal/VOC/voc2007/index.html>.

Code availability

The source code for the metrics will be made publicly available upon publication.

Appendix A Comprehensive Attack Survey Data

The following tables provide the comprehensive data for our survey of adversarial attacks (Section 2.2). As discussed in Section 2.5, this data highlights the fragmentation in the field. Table A1 details the disparate outcomes, perturbation costs, metrics, detectors, and datasets reported in the original articles for a wide range of attacks.

Appendix B Benchmark Perceptibility Metrics

In Table B4 we provide the detailed numerical data for the perceptibility analysis in Section 3.2.1. It lists the mean and standard deviation for L_2 , L_∞ , SSIM, and LPIPS for each attack evaluated in our benchmark.

Appendix C Detailed Adversarial Training Results (YOLOv3)

The full experimental results for the YOLOv3 detector discussed in Section 4 are presented in Table C5. This table details the mAP performance of YOLOv3 models fine-tuned on various single-attack and mixed-attack datasets, evaluated against the complete suite of benchmark attacks.

Appendix D Detailed Adversarial Training Results (Faster R-CNN)

The full experimental results for the Faster R-CNN detector after adversarial training (cf. 4) are presented in Table D6, followed by a granular breakdown of performance for the main experiments in Tables D7, D8, and D9.

Table A1 Examples of adversarial attacks for object detection. * denotes if the code is publicly available. Inspired by Nguyen et al. (2025).

NAME	OUTCOME	SPECIFICITY	LOCALITY	PERTURBATION COST	METRICS	DETECTORS USED	DATASET USED
AdvART (Guesmi et al., 2024)	Vanishing	Universal	Patch	SSIM	mAP, Success rate	YOLOv4tiny, YOLOv3tiny, YOLOv4, YOLOv3	INRIA, MPII
LGP (G. Li et al., 2024)*	Random	Image-specific	Entire image	FID, IW-SSIM, PSNR-B	mAP, Number of attacked targets per image, Success rate	Faster R-CNN, Def-DETR, VFNet, Cascade R-CNN, Rotated FCOS,...	COCO, DOTA-v1.0
OSFD (Ding et al., 2024)*	Random	Image-specific	Entire image	L_∞	mAP	Faster R-CNN, YOLOv3, YOLOv4tiny, YOLOv3tiny, (Also tested on: DETR, YOLOF, YOLOX, FCOS)	VOCC2012
Patch-based FP (Tang et al., 2024)	Fabrication	Universal	Patch	-	mAP, Average instances created, Average Precision Decrease, Average Score Created, FP Rate Increase	DOTA-v1.0, RSOD, NWPU VHR-10	
ShiftAttack (H. Li et al., 2024)	Other	Image-specific	Entire image	L_2 , SSIM	Success rate	YOLOv3, YOLOv5, YOLOv8, ATSS, FoveaBox, FreeAnchor, GFL, RetinaNet, RTMDet, Swin-Transformer, DDDQ, Def-DETR	COCO, VOCC2012, VOCC2012
Targeted context attack (C. Sun et al., 2024)	Mislabeling	Image-specific	Entire image	L_∞	Success rate	Faster R-CNN, YOLOv3 (Also tested on: Libra, FoveaBox, FreeAnchor, DETR, Def-DETR)	COCO, VOCC2007
ASC (Y. Zhang et al., 2023)	Vanishing	Image-specific	Entire image	L_0	Success rate	SSD12, YOLOv3, YOLOX, Faster R-CNN, Mask R-CNN, DAB-DETR, DAB-DETR	COCO, Cityscapes, BDD100K
EBAD (Cai et al., 2023)*	Mislabeling	Image-specific	Entire image	L_∞	Success rate	Faster R-CNN, YOLOv3, FCOS, SSD, Grid R-CNN (Also tested on: RetinaNet, Libra, FoveaBox, FreeAnchor, DETR, Def-DETR)	COCO, VOCC2007
Patches against UAV (Shrestha et al., 2023)*	Vanishing	Universal	Patch	-	mAP, Success rate	YOLOv5s, YOLOv3, YOLOv4	VisDrone-2019
Phantom Sponges (Shapira et al., 2023)	Fabrication, Inference latency	Universal	Entire image	L_2	Number of created objects, time, recall	BDD100K, MTSDF, LISA, VOC	
T-SEA (H. Huang et al., 2023)*	Vanishing	Universal	Patch	-	AP (for person)	Faster R-CNN, YOLOv2, YOLOv3, YOLOv3-tiny, YOLOv4, YOLOv4-tiny, YOLOv5, SSD	INRIA, COCO-person, CCTV-person
ADC (Yin et al., 2022)	Mislabeling, Vanishing, Fabrication	Image-specific	Entire image	L_∞	Success rate	Faster R-CNN	COCO, VOCC2007, VOCC2012

Continued on next page

Table A1 - continued from previous page
Table A2 *

NAME	OUTCOME	SPECIFICITY	LOCALITY	PERTURBATION COST	METHICS	DETECTORS USED	DATASET USED
Adversarial Texture (Z. Hu et al., 2022)*	Vanishing	Universal	Patch	-	AP	Faster R-CNN, YOLOv2, YOLOv3, Mask R-CNN	INRIA, Custom dataset
CAA (Cai, Xie, et al., 2022)*	Mislabeling	Image-specific	Entire image	L_∞	Success rate	Faster R-CNN, YOLOv3, RetinaNet (Also tested on: FCOS, Libra, FoveaBox, FreeAnchor, DETR, Def-DETR, YOLOv3, SSD, RetinaNet)	COCO, VOC2007
Daedalus (D. Wang et al., 2021)*	Fabrication	Image-specific	Entire image	L_0, L_2	mAP, FP rate	SSD, YOLOv3, RetinaNet, Faster R-CNN, Mask R-CNN, Cascade R-CNN, Cascade Mask R-CNN, Hybrid Task Cascade, EfficientDet	COCO
RAD (S. Chen et al., 2022)*	Random	Image-specific	Entire image	L_∞	mAP, Accuracy, Mean Average Recall	Faster R-CNN, Libra, RetinaNet, FoveaBox	COCO
ZQA (Cai, Rane, et al., 2022)	Mislabeling	Image-specific	Entire image	L_∞	Success rate	YOLOv2, YOLOv3, YOLOv3-tiny, YOLOv4, YOLOv4-tiny, Faster R-CNN	INRIA, MPII, Custom dataset
Naturalistic Patches (Y.-C.-T. Hu et al., 2021)*	Vanishing	Universal	Patch	-	mAP	COCO, VOC2007	Visual Genome
Pick-Object Attack (Nezami et al., 2021)*	Mislabeling	Image-specific	Entire image	L_2 , SSIM	mAP, Success rate, Average Confidence of True Class, Average Confidence of Adversarial Class	Faster R-CNN	COCO, Visual Genome
PRFA (Liang et al., 2021)*	Random	Image-specific	Patch	-	AP	map, Average queries	COCO
RPAttack (H. Huang et al., 2021)*	Vanishing	Image-specific	Patch	-	AP	Faster R-CNN, YOLOv4	COCO, VOC2007
U-DOS (D. Li et al., 2021)	Vanishing	Universal	Entire image	L_∞	mAP, Blind degree	Faster R-CNN, SSD, YOLO	VOC2007, VOC2012, Caltech Pedestrian
CAP (H. Zhang et al., 2020)	Vanishing	Image-specific	Entire image	Peak Signal-to-Noise Ratio	mAP, Recall	Faster R-CNN	COCO, VOC2007
Contextual Adversarial Patches (Saha et al., 2020)*	Vanishing	Image-specific, Universal	Patch	-	mAP	YOLOv2	VOC2007, KITTI

Table A1 - continued from previous page

Table A3 *

NAME	OUTCOME	SPECIFICITY	LOCALITY	PERTURBATION COST	METRICS	DETECTORS USED	DATASET USED
DPAttack (S. Wu et al., 2020)*	Vanishing	Image-specific	Patch	-	AP	Faster R-CNN, YOLOv4	COCO
Evaporate Attack (Y. Wang et al., 2020)	Vanishing	Image-specific	Entire image	L_2	Success rate, False negative increase	YOLOv3, SSD, Faster R-CNN	COCO, VOC2007
FB Invisible cloak (Z. Wu et al., 2020)	Vanishing	Universal	Patch	-	AP	YOLOv2, YOLOv3, Faster R-CNN	COCO, VOC2007, INRIA, Custom dataset
TOG (Chow et al., 2020)*	Random, Vanishing, Fabrication, Mislabeling	Image-specific, Universal	Entire image, Patch	L_∞	mAP, % of vanished objects	Faster R-CNN, SSD, YOLOv3	COCO, VOC2007, INRIA
UPC (L. Huang et al., 2020)*	Mislabeling	Universal	Patch (on object)	-	AP	Faster R-CNN	VOC2007, VOC2012, Custom dataset
Adversarial T-shirt (Xu et al., 2020)*	Vanishing	Universal	Patch	-	Success rate	Faster R-CNN, YOLOv2	Custom dataset
Patches to attack person detection (Thys et al., 2019)*	Vanishing	Universal	Patch	-	Recall	YOLOv2	INRIA
Seeing isn't Believing (Zhao et al., 2019)	Vanishing, Fabrication	Image-specific	Patch	-	Success rate	Faster R-CNN, YOLOv3 (Also tested on: SSD, RPN, Mask R-CNN)	Custom dataset
ShapeShifter (S.-T. Chen et al., 2018)*	Mislabeling	Image-specific	Patch (on object)	L_∞	Success rate (for stop sign)	Faster R-CNN	COCO
DPatch (X. Liu et al., 2018)*	Random	Image-specific	Patch	-	mAP	Faster R-CNN, YOLO	VOC2007
Imperceptible background patches (Y. Li, Bian, & Lyu, 2018)	Random	Image-specific	Patch	-	mAP	True Positive Class Loss, True Positive Shape Loss, False Positive Class Loss	COCO
Invisible cloak (D.Y. Yang et al., 2018)	Vanishing	Universal	Patch	-	Precision	Tiny YOLO	Custom dataset
R-AP (Y. Li, Tian, et al., 2018)*	Random	Image-specific	Entire image	-	Peak Signal-to -Noise Ratio _o	mAP	Faster R-CNN, Region Fully Convolutional Network
UEA (Wei et al., 2019)*	Random	Image-specific	Entire image	-	mAP	Faster R-CNN, SSD	VOC2007, ImageNet VID
DAG (Xie et al., 2017)*	Mislabeling	Image-specific	Entire image	-	mAP, mIoU	Faster R-CNN, FCN	VOC2007, Cityscapes

Table B4 Imperceptibility (L_2 , L_∞ , LPIPS) / Similarity (SSIM) of attacks between original and adversarial images (mean \pm std), depending on the surrogate model (Less perceptible in bold, second less perceptible underlined). For EBAD victim models are identical to surrogates. Note: For OSFD, L_2 , LPIPS, and SSIM were computed after resizing images back to their original dimensions. The L_∞ norm is reported at the attack’s native resolution, as this is where its constraint is applied

Attack	Surrogate Model	$L_2 \downarrow$	$L_\infty \downarrow$	SSIM \uparrow	LPIPS \downarrow
CAA $\epsilon = 10$	F. R-CNN & YOLOv3	4797.01 \pm 379.45	43.53 \pm 18.08	<u>0.84</u> \pm 0.06	<u>0.13</u> \pm 0.08
CAA $\epsilon = 30$	F. R-CNN & YOLOv3	9464.09 \pm 717.02	56.11 \pm 15.54	0.63 \pm 0.11	0.31 \pm 0.13
EBAD $\epsilon = 10$	F. R-CNN & YOLOv3	4223.71 \pm 385.10	<u>10.0</u> \pm 0.0	0.86 \pm 0.06	0.11 \pm 0.07
EBAD $\epsilon = 30$	F. R-CNN & YOLOv3	12339.27 \pm 1169.83	30.0 \pm 0.0	0.53 \pm 0.13	0.40 \pm 0.14
EBAD $\epsilon = 50$	F. R-CNN & YOLOv3	20281.73 \pm 2065.19	50.0 \pm 0.0	0.37 \pm 0.12	0.62 \pm 0.16
OSFD	YOLOv3	8255.96 \pm 3090.36	7.0 \pm 0.0	0.81 \pm 0.04	0.20 \pm 0.08
OSFD	F. R-CNN	7707.84 \pm 3080.61	7.0 \pm 0.0	0.83 \pm 0.05	0.17 \pm 0.08
Phantom Sponges	YOLOv3	9745.94 \pm 1258.09	89.96 \pm 14.38	0.74 \pm 0.08	0.23 \pm 0.10

Table C5 The mAP (%) metric of the **YOLOv3** detectors after adversarial training. When only one attack and its percentage are given, the rest of the adversarial training dataset is filled with unattacked images. The number next to CAA and EBAD indicates the value of their respective parameters ϵ . The Benign column concerns the original images. F. R-CNN is short for Faster R-CNN.

FINE-TUNED ON	Benign	CAA $\epsilon = 10$	CAA $\epsilon = 20$	CAA $\epsilon = 30$	EBAD $\epsilon = 10$	EBAD $\epsilon = 20$	EBAD $\epsilon = 30$	OSFD $k = 1$ YOLOv3	OSFD $k = 2$ YOLOv3	OSFD $k = 3$ YOLOv3	OSFD F. R-CNN	Phantom Sponges YOLOv3
Baseline		75.8	12.3	7.3	6.0	22.0	19.3	18.1	20.2	8.1	6.6	22.4
Benign		75.8	28.0	19.4	17.1	48.7	32.7	28.1	22.4	9.9	8.3	23.3
CAA ₃₀		72.2	72.2	69.3	66.3	72.1	67.4	60.6	59.8	54.0	53.0	61.6
CAA ₃₀ 75%		72.8	71.6	68.6	64.2	71.0	67.2	61.3	59.1	51.1	49.4	60.4
CAA ₃₀ 50%		73.6	69.5	65.5	61.1	69.8	65.1	59.4	53.1	43.6	41.4	54.9
CAA ₃₀ 25%		74.2	62.8	56.2	49.5	65.8	60.6	54.0	39.4	25.4	23.0	41.0
EBAD ₁₀		75.4	67.0	48.3	38.1	70.1	51.8	39.3	48.9	38.3	36.9	53.2
EBAD ₁₀ 75%		74.4	63.6	45.2	38.2	69.1	51.2	38.4	46.0	33.6	31.4	48.9
EBAD ₁₀ 50%		73.7	63.1	45.0	36.7	67.1	52.2	41.2	44.2	32.5	30.4	48.2
EBAD ₁₀ 25%		75.0	50.1	32.9	28.6	63.1	44.2	35.7	34.6	20.5	18.4	37.4
OSFD		73.5	73.9	69.6	65.1	73.6	65.2	53.5	71.1	69.7	69.1	69.8
OSFD 75%		72.8	72.3	67.7	61.8	72.4	63.2	51.3	70.0	68.1	67.8	68.6
OSFD 50%		71.8	71.2	66.4	60.5	71.6	62.5	51.1	69.0	66.5	66.0	67.1
OSFD 25%		74.1	70.6	63.0	56.3	71.4	60.2	48.0	68.5	65.0	64.1	66.7
OSFD 50% CAA ₃₀ 50%		72.2	72.9	70.9	67.6	72.8	67.6	59.5	69.2	67.6	67.2	68.5
OSFD 75% CAA ₃₀ 25%		73.1	73.5	71.3	67.5	73.6	67.6	58.4	<u>70.7</u>	68.9	68.2	<u>69.3</u>
SFD 33% CAA ₃₀ 33%		71.7	72.1	69.3	65.6	71.8	67.0	59.0	68.5	66.3	65.9	67.4
Benign 34%												66.0
PhantomSponges		74.1	62.6	44.1	35.4	67.6	48.0	36.2	40.7	28.8	27.3	45.2
PhantomSponges 75%		75.8	57.4	39.2	29.7	64.8	44.8	34.6	37.2	23.8	21.7	39.8
PhantomSponges 50%		75.5	52.1	34.7	25.3	60.7	42.0	32.4	32.6	20.0	17.9	35.2
PhantomSponges 25%		75.9	37.4	24.9	22.3	56.4	36.5	30.6	26.7	13.5	11.9	28.8
EBAD ₅₀		68.7	69.4	68.9	66.8	70.0	68.8	<u>66.0</u>	55.5	50.1	49.4	57.7
EBAD ₅₀ 50% OSFD 50%		71.9	72.6	<u>71.6</u>	<u>69.5</u>	73.0	69.7	65.2	69.6	67.7	67.2	68.7
EBAD ₅₀ 75% OSFD 25%		70.8	71.8	71.3	<u>69.5</u>	71.9	<u>69.9</u>	66.2	67.9	65.9	65.5	67.0
EBAD ₅₀ 25% OSFD 75%		73.0	<u>73.7</u>	71.9	69.6	<u>73.5</u>	70.0	64.8	71.1	<u>69.3</u>	<u>68.9</u>	69.8

Table D6 The **mAP(%)** metric of the **Faster R-CNN** detectors after adversarial training. When only one attack and its percentage are given, the rest of the adversarial dataset is filled with unattacked images. The number next to CAA and EBAD indicates the value of their respective parameters ϵ . The Benign column concerns the original images. F. R-CNN is short for Faster R-CNN.

	FINE-TUNED ON	Benign	CAA $\epsilon = 10$	CAA $\epsilon = 20$	EBAD $\epsilon = 10$ F. R-CNN	EBAD $\epsilon = 30$ F. R-CNN	EBAD $\epsilon = 50$ F. R-CNN	OSFD $k = 3$ YOLOv3	OSFD F. R-CNN	Phantom Sponges YOLOv3
Baseline		79.3	8.7	3.9	3.4	28.9	26.1	24.9	7.4	3.4
Benign		80.4	19.8	9.3	8.0	38.0	31.8	30.2	6.9	3.6
CAA ₃₀		76.9	74.4	71.7	70.3	72.3	65.5	59.0	38.2	38.0
CAA ₃₀ 75%		77.8	<u>73.8</u>	70.4	68.9	70.0	64.3	59.0	31.2	29.6
CAA ₃₀ 50%		78.8	72.8	69.1	67.4	66.2	63.4	59.2	23.1	20.4
CAA ₃₀ 25%		<u>79.6</u>	70.3	66.5	64.5	59.8	60.4	56.9	16.9	12.9
EBAD ₁₀		76.7	73.7	69.5	67.5	72.6	63.7	55.7	35.2	35.4
EBAD ₁₀ 75%		77.4	72.6	68.5	66.4	71.9	64.2	57.4	32.5	32.6
EBAD ₁₀ 50%		78.1	72.1	67.1	64.7	70.6	63.7	57.6	27.3	27.4
EBAD ₁₀ 25%		79.0	70.3	63.9	60.8	67.3	61.0	53.1	21.1	19.6
OSFD		74.5	72.6	67.6	65.5	72.3	61.0	51.5	65.1	67.4
OSFD 75%		75.7	72.4	68.2	65.9	71.9	62.6	54.1	63.7	65.8
OSFD 50%		76.6	71.6	67.4	65.2	70.8	62.7	55.8	61.2	63.3
OSFD 25%		77.8	71.0	65.6	63.4	69.0	61.9	55.7	56.6	58.0
OSFD 50% CAA ₃₀ 50%		74.6	73.7	<u>71.4</u>	<u>70.0</u>	73.5	64.8	54.7	62.8	64.5
OSFD 75% CAA ₃₀ 25%		74.5	73.5	70.5	69.1	<u>73.2</u>	64.0	54.2	<u>64.4</u>	<u>66.2</u>
OSFD 33% CAA ₃₀ 33%		76.0	73.1	70.1	68.4	71.9	63.7	55.1	60.5	62.0
Benign 34%										69.5
PhantomSponges		78.1	49.4	25.8	19.5	46.2	36.7	33.9	10.9	7.9
PhantomSponges 75%		79.5	45.6	21.9	16.6	44.2	35.8	33.4	10.0	6.6
PhantomSponges 50%		80.0	41.1	18.9	14.7	43.2	35.5	33.2	9.6	5.9
PhantomSponges 25%		80.3	33.3	14.9	12.1	41.2	34.5	32.6	8.5	4.8
EBAD ₅₀		74.9	72.0	69.5	68.6	72.2	68.4	<u>64.5</u>	33.3	33.7
EBAD ₅₀ 50% OSFD 50%		73.5	71.9	70.0	69.1	73.0	<u>68.7</u>	63.7	61.7	63.6
EBAD ₅₀ 75% OSFD 25%		72.4	70.9	69.2	68.7	72.3	68.9	64.8	58.8	60.6
EBAD ₅₀ 25% OSFD 75%		74.3	72.5	70.0	68.8	73.1	67.5	62.1	63.7	65.8

Table D7 Performance (mAP in %) of Faster R-CNN detectors defended by adversarial training. The subscript next to CAA and EBAD indicates their respective ϵ parameters. For EBAD attacks, the target model is Faster R-CNN. For OSFD and Phantom Sponges, the model mentioned is the surrogate used for attack generation. Higher is better.

FINE-TUNED ON	Benign	CAA ₁₀	CAA ₃₀	EBAD ₁₀	EBAD ₃₀	EBAD ₅₀	OSFD	OSFD	Phantom Sponges
						YOLOv3	F. R-CNN	YOLOv3	
Baseline	<u>79.3</u>	8.7	3.4	28.9	26.1	24.9	7.4	3.4	65.7
Benign	80.4	19.8	8.0	38.0	31.8	30.2	6.9	3.6	65.1
CAA ₃₀	76.9	74.4	70.3	<u>72.3</u>	<u>65.5</u>	<u>59.0</u>	<u>38.2</u>	<u>38.0</u>	<u>70.0</u>
EBAD ₁₀	76.7	<u>73.7</u>	67.5	72.6	63.7	55.7	35.2	35.4	69.4
EBAD ₅₀	74.9	72.0	<u>68.6</u>	72.2	68.4	64.5	33.3	33.7	67.5
OSFD	74.5	72.6	65.5	<u>72.3</u>	61.0	51.5	65.1	67.4	68.0
Phantom Sponges	78.1	49.4	19.5	46.2	36.7	33.9	10.9	7.9	75.0

Table D8 Performance (\mathbf{AP}_{10c} in %) of Faster R-CNN detectors defended by adversarial training. The subscript next to CAA and EBAD indicates their respective ϵ parameters. For EBAD attacks, the target model is Faster R-CNN. For OSFD and Phantom Sponges, the model mentioned is the surrogate used for attack generation. Higher is better.

FINE-TUNED ON	Benign	CAA ₁₀	CAA ₃₀	EBAD ₁₀	EBAD ₃₀	EBAD ₅₀	OSFD	OSFD YOLOv3	F. R-CNN	YOLOv3	Phantom Sponges
Baseline	82.7	37.3	33.3	67.4	66.1	65.4	4.0	2.1	73.3		
Benign	84.7	45.3	36.1	69.3	68.2	67.7	4.7	2.5	73.1		
CAA ₃₀	82.3	80.3	77.5	78.6	<u>74.8</u>	<u>72.5</u>	<u>45.9</u>	<u>45.4</u>	<u>76.5</u>		
EBAD ₁₀	82.4	<u>80.0</u>	75.9	79.4	<u>74.8</u>	72.1	42.3	43.1	76.0		
EBAD ₅₀	81.1	79.0	<u>76.9</u>	<u>79.0</u>	76.7	74.9	40.9	41.0	74.9		
OSFD	80.1	78.4	74.2	78.1	72.2	69.0	72.4	74.6	74.7		
Phantom Sponges	<u>83.0</u>	65.1	44.1	69.4	67.9	67.7	9.6	6.8	79.9		

Table D9 Performance (CSR in %) of Faster R-CNN detectors defended by adversarial training. The subscript next to CAA and EBAD indicates their respective ϵ parameters. For EBAD attacks, the target model is Faster R-CNN. For OSFD and Phantom Sponges, the model mentioned is the surrogate used for attack generation. Higher is better.

FINE-TUNED ON	Benign	CAA ₁₀	CAA ₃₀	EBAD ₁₀	EBAD ₃₀	OSFD	OSFD	Phantom Sponges
					YOLOv3	F. R-CNN	YOLOv3	
Baseline	89.8	27.4	17.3	51.6	51.0	30.5	24.3	80.8
Benign	89.8	44.1	24.9	54.2	52.7	28.2	22.2	77.4
CAA ₃₀	88.5	<u>85.9</u>	81.4	82.9	<u>77.6</u>	<u>72.3</u>	<u>65.8</u>	<u>67.1</u>
EBAD ₁₀	88.7	86.0	79.7	83.9	76.6	70.2	64.0	66.5
EBAD ₅₀	87.7	84.6	<u>81.1</u>	<u>83.1</u>	80.2	77.1	62.9	64.8
OSFD	86.6	84.0	77.2	82.8	73.4	66.0	80.5	82.0
Phantom Sponges	<u>89.1</u>	67.5	45.1	61.9	55.2	53.8	39.4	37.5
								85.5

References

Amirkhani, A., & Karimi, M.P. (2022). Adversarial defenses for object detectors based on Gabor convolutional layers. *The visual computer*, 38(6), 1929–1944,

Amirkhani, A., Karimi, M.P., Banitalebi-Dehkordi, A. (2023). A survey on adversarial attacks and defenses for object detection and their applications in autonomous vehicles. *The Visual Computer*, 39(11), 5293–5307,

Bai, S., Li, Y., Zhou, Y., Li, Q., Torr, P.H. (2020). Adversarial metric attack and defense for person re-identification. *IEEE Transactions on Pattern Analysis and Machine Intelligence*, 43(6), 2119–2126,

Bochkovskiy, A., Wang, C.-Y., Liao, H.-Y.M. (2020). YOLOv4: Optimal speed and accuracy of object detection. *arXiv preprint arXiv:2004.10934*, ,

Bolya, D., Foley, S., Hays, J., Hoffman, J. (2020). TIDE: A general toolbox for identifying object detection errors. *European Conference on Computer Vision (ECCV)*.

Bouniot, Q., Audigier, R., Loesch, A. (2020). Vulnerability of person re-identification models to metric adversarial attacks. *Proceedings of the IEEE/CVF Conference on Computer Vision and Pattern Recognition (CVPR) Workshops*.

Cai, Z., Rane, S., Brito, A.E., Song, C., Krishnamurthy, S.V., Roy-Chowdhury, A.K., Asif, M.S. (2022). Zero-query transfer attacks on context-aware object detectors. *Proceedings of the IEEE/CVF Conference on Computer Vision and Pattern Recognition (CVPR)*.

Cai, Z., Tan, Y., Asif, M.S. (2023). Ensemble-based blackbox attacks on dense prediction. *Proceedings of the IEEE/CVF Conference on Computer Vision and Pattern Recognition (CVPR)*.

Cai, Z., & Vasconcelos, N. (2018). Cascade R-CNN: Delving into high quality object detection. *Proceedings of the IEEE/CVF Conference on Computer Vision and Pattern Recognition (CVPR)*.

Cai, Z., Xie, X., Li, S., Yin, M., Song, C., Krishnamurthy, S.V., ... Asif, M.S. (2022). Context-aware transfer attacks for object detection. *Proceedings of the AAAI Conference on Artificial Intelligence*.

Carion, N., Massa, F., Synnaeve, G., Usunier, N., Kirillov, A., Zagoruyko, S. (2020). End-to-end object detection with transformers. *European Conference*

on Computer Vision (ECCV).

Chakraborty, A., Alam, M., Dey, V., Chattopadhyay, A., Mukhopadhyay, D. (2021). A survey on adversarial attacks and defences. *CAAI Transactions on Intelligence Technology*, 6(1), 25–45,

Chen, K., Wang, J., Pang, J., Cao, Y., Xiong, Y., Li, X., ... Lin, D. (2019). MMDetection: Open MMLab detection toolbox and benchmark. *arXiv preprint arXiv:1906.07155*, ,

Chen, P.-C., Kung, B.-H., Chen, J.-C. (2021). Class-aware robust adversarial training for object detection. *Proceedings of the IEEE/CVF Conference on Computer Vision and Pattern Recognition (CVPR)*.

Chen, S., He, F., Huang, X., Zhang, K. (2022). Relevance attack on detectors. *Pattern Recognition*, 124, 108491,

Chen, S.-T., Cornelius, C., Martin, J., Chau, D.H. (2018). ShapeShifter: Robust physical adversarial attack on Faster R-CNN object detector. *Joint European Conference on Machine Learning and Knowledge Discovery in Databases (ECML PKDD)*.

Chiang, P.-y., Curry, M., Abdelkader, A., Kumar, A., Dickerson, J., Goldstein, T. (2020). Detection as regression: Certified object detection with median smoothing. *Advances in Neural Information Processing Systems (NeurIPS)*, ,

Chow, K.-H., Liu, L., Loper, M., Bae, J., Gursoy, M.E., Truex, S., ... Wu, Y. (2020). Adversarial objectness gradient attacks in real-time object detection systems. *2020 Second IEEE International Conference on Trust, Privacy and Security in Intelligent Systems and Applications (TPS-ISA)*.

Costa, J.C., Roxo, T., Proen  a, H., Inacio, P.R.M. (2024). How deep learning sees the world: A survey on adversarial attacks & defenses. *IEEE Access*, 12, 61113–61136,

Ding, X., Chen, J., Yu, H., Shang, Y., Qin, Y., Ma, H. (2024). Transferable adversarial attacks for object detection using object-aware significant feature distortion. *Proceedings of the AAAI Conference on Artificial Intelligence*.

Dong, Z., Wei, P., Lin, L. (2022). Adversarially-aware robust object detector. *European Conference on Computer Vision (ECCV)*.

Duan, K., Bai, S., Xie, L., Qi, H., Huang, Q., Tian, Q. (2019). CenterNet: Key-point triplets for object detection. *Proceedings of the IEEE/CVF International Conference on Computer Vision (ICCV)*.

Everingham, M., Van Gool, L., Williams, C.K., Winn, J., Zisserman, A. (2010). The Pascal Visual Object Classes (VOC) challenge. *International journal of computer vision*, 88(2), 303–338,

Fujii, K., Kera, H., Kawamoto, K. (2022). Adversarially trained object detector for unsupervised domain adaptation. *IEEE Access*, 10, 59534–59543,

Ge, Z., Liu, S., Wang, F., Li, Z., Sun, J. (2021). Yolox: Exceeding yolo series in 2021. *arXiv preprint arXiv:2107.08430*, ,

Gong, Y., Zhong, Z., Qu, Y., Luo, Z., Ji, R., Jiang, M. (2024). Cross-modality perturbation synergy attack for person re-identification. *Advances in Neural Information Processing Systems (NeurIPS)*, ,

Goodfellow, I.J., Shlens, J., Szegedy, C. (2015). Explaining and harnessing adversarial examples. Y. Bengio & Y. LeCun (Eds.), *3rd International Conference on Learning Representations, (ICLR)*.

Guesmi, A., Bilasco, I.M., Shafique, M., Alouani, I. (2024). AdvART: Adversarial art for camouflaged object detection attacks. *2024 IEEE International Conference on Image Processing (ICIP)*.

He, K., Gkioxari, G., Dollár, P., Girshick, R. (2017). Mask R-CNN. *Proceedings of the IEEE international conference on computer vision (ICCV)*.

He, K., Zhang, X., Ren, S., Sun, J. (2016). Deep residual learning for image recognition. *Proceedings of the IEEE/CVF Conference on Computer Vision and Pattern Recognition (CVPR)*.

Hoiem, D., Chodpathumwan, Y., Dai, Q. (2012). Diagnosing error in object detectors. *European Conference on Computer Vision* .

Hu, Y.-C.-T., Kung, B.-H., Tan, D.S., Chen, J.-C., Hua, K.-L., Cheng, W.-H. (2021). Naturalistic physical adversarial patch for object detectors. *Proceedings of the IEEE/CVF International Conference on Computer Vision (ICCV)*.

Hu, Z., Huang, S., Zhu, X., Sun, F., Zhang, B., Hu, X. (2022). Adversarial texture for fooling person detectors in the physical world. *Proceedings of the IEEE/CVF Conference on Computer Vision and Pattern Recognition (CVPR)*.

Huang, H., Chen, Z., Chen, H., Wang, Y., Zhang, K. (2023). T-SEA: Transfer-based self-ensemble attack on object detection. *Proceedings of the IEEE/CVF Conference on Computer Vision and Pattern Recognition (CVPR)*.

Huang, H., Wang, Y., Chen, Z., Tang, Z., Zhang, W., Ma, K.-K. (2021). RPAttack: Refined patch attack on general object detectors. *2021 IEEE International Conference on Multimedia and Expo (ICME)*.

Huang, L., Gao, C., Zhou, Y., Xie, C., Yuille, A.L., Zou, C., Liu, N. (2020). Universal physical camouflage attacks on object detectors. *Proceedings of the IEEE/CVF Conference on Computer Vision and Pattern Recognition (CVPR)*.

Jing, L., Wang, R., Ren, W., Dong, X., Zou, C. (2024). PAD: Patch-agnostic defense against adversarial patch attacks. *Proceedings of the IEEE/CVF Conference on Computer Vision and Pattern Recognition (CVPR)*.

Khodabandeh, M., Vahdat, A., Ranjbar, M., Macready, W.G. (2019). A robust learning approach to domain adaptive object detection. *Proceedings of the IEEE/CVF International Conference on Computer Vision (ICCV)* (pp. 480–490).

Kim, T., Yu, Y., Ro, Y.M. (2022). Defending physical adversarial attack on object detection via adversarial patch-feature energy. *Proceedings of the 30th ACM International Conference on Multimedia*.

Li, D., Zhang, J., Huang, K. (2021). Universal adversarial perturbations against object detection. *Pattern Recognition*, 110, 107584,

Li, G., Xu, Y., Ding, J., Xia, G.-S. (2024). Toward generic and controllable attacks against object detection. *IEEE Transactions on Geoscience and Remote Sensing*, 62, 1–12,

Li, H., Yang, Z., Gong, M., Chen, S., Qin, A., Niu, Z., . . . Zhou, Y. (2024). ShiftAttack: Toward attacking the localization ability of object detector. *IEEE Transactions on Circuits and Systems for Video Technology*, ,

Li, S., Zhu, S., Paul, S., Roy-Chowdhury, A., Song, C., Krishnamurthy, S., . . . Chan, K.S. (2020). Connecting the dots: Detecting adversarial perturbations using context inconsistency. *European Conference on Computer Vision (ECCV)*.

Li, X., Chen, H., Hu, X. (2025). On the importance of backbone to the adversarial robustness of object detectors. *IEEE Transactions on Information Forensics and Security*, ,

Li, Y., Bian, X., Lyu, S. (2018). Attacking object detectors via imperceptible patches on background. *arXiv preprint arXiv:1809.05966*, 1, ,

Li, Y., Tian, D., Chang, M.-C., Bian, X., Lyu, S. (2018). Robust adversarial perturbation on deep proposal-based models. *British machine vision conference 2018, BMVC*.

Liang, S., Wu, B., Fan, Y., Wei, X., Cao, X. (2021). Parallel rectangle flip attack: A query-based black-box attack against object detection. *Proceedings of the IEEE/CVF International Conference on Computer Vision (ICCV)*.

Lin, T.-Y., Goyal, P., Girshick, R., He, K., Dollar, P. (2017). Focal loss for dense object detection. *Proceedings of the IEEE International Conference on Computer Vision (ICCV)*.

Lin, T.-Y., Maire, M., Belongie, S., Hays, J., Perona, P., Ramanan, D., ... Zitnick, C.L. (2014). Microsoft COCO: Common objects in context. *European Conference on Computer Vision (ECCV)*.

Liu, J., Levine, A., Lau, C.P., Chellappa, R., Feizi, S. (2022). Segment and Complete: Defending Object detectors against adversarial patch attacks with robust patch detection. *Proceedings of the IEEE/CVF Conference on Computer Vision and Pattern Recognition (CVPR)*.

Liu, W., Anguelov, D., Erhan, D., Szegedy, C., Reed, S., Fu, C.-Y., Berg, A.C. (2016). SSD: Single shot MultiBox detector. *European Conference on Computer Vision (ECCV)* (pp. 21–37).

Liu, X., Yang, H., Song, L., Li, H., Chen, Y. (2018). DPatch: Attacking object detectors with adversarial patches. *CoRR, abs/1806.02299*, 2, 1,

Liu, Z., Lin, Y., Cao, Y., Hu, H., Wei, Y., Zhang, Z., ... Guo, B. (2021). Swin transformer: Hierarchical vision transformer using shifted windows. *Proceedings of the IEEE/CVF International Conference on Computer Vision (ICCV)*.

Metzen, J.H., Finnie, N., Hutmacher, R. (2021). Meta adversarial training against universal patches. *arXiv preprint arXiv:2101.11453*, ,

Miller, D.J., Xiang, Z., Kesidis, G. (2020). Adversarial learning targeting deep neural network classification: A comprehensive review of defenses against attacks. *Proceedings of the IEEE, 108(3)*, 402–433,

Nezami, O.M., Chaturvedi, A., Dras, M., Garain, U. (2021). Pick-Object-Attack: Type-specific adversarial attack for object detection. *Computer Vision and Image Understanding*, 211, 103257,

Nguyen, K.N.T., Zhang, W., Lu, K., Wu, Y.-H., Zheng, X., Li Tan, H., Zhen, L. (2025). A survey and evaluation of adversarial attacks in object detection. *IEEE Transactions on Neural Networks and Learning Systems*, 36(9), 15706-15722,

Nie, W., Guo, B., Huang, Y., Xiao, C., Vahdat, A., Anandkumar, A. (2022). Diffusion models for adversarial purification. *Proceedings of the 39th International Conference on Machine Learning (ICML)*.

Pang, J., Chen, K., Shi, J., Feng, H., Ouyang, W., Lin, D. (2019). Libra R-CNN: Towards balanced learning for object detection. *Proceedings of the IEEE/CVF Conference on Computer Vision and Pattern Recognition (CVPR)*.

Redmon, J., & Farhadi, A. (2018). Yolov3: An incremental improvement. *arXiv preprint arXiv:1804.02767*, ,

Ren, S., He, K., Girshick, R., Sun, J. (2015). Faster R-CNN: Towards real-time object detection with region proposal networks. *Advances in neural information processing systems (NeurIPS)*, ,

Saha, A., Subramanya, A., Patil, K., Pirsiavash, H. (2020). Role of spatial context in adversarial robustness for object detection. *Proceedings of the IEEE/CVF Conference on Computer Vision and Pattern Recognition (CVPR) Workshops*.

Shapira, A., Zolfi, A., Demetrio, L., Biggio, B., Shabtai, A. (2023). Phantom Sponges: Exploiting non-maximum suppression to attack deep object detectors. *Proceedings of the IEEE/CVF Winter Conference on Applications of Computer Vision (WACV)*.

Shrestha, S., Pathak, S., Viegas, E.K. (2023). Towards a robust adversarial patch attack against unmanned aerial vehicles object detection. *2023 IEEE/RSJ International Conference on Intelligent Robots and Systems (IROS)*.

Sun, C., Zhang, X., Han, H., Sun, H. (2024). Targeted context attack for object detection. *Neurocomputing*, 601, 128208,

Sun, P., Zhang, R., Jiang, Y., Kong, T., Xu, C., Zhan, W., ... Luo, P. (2021). Sparse R-CNN: End-to-end object detection with learnable proposals. *Proceedings of the IEEE/CVF Conference on Computer Vision and Pattern Recognition (CVPR)*.

Tang, G., Yao, W., Jiang, T., Zhao, Y., Sun, J. (2024). Adversarial patch-based false positive creation attacks against aerial imagery object detectors. *Neurocomputing*, 579, 127431,

Tarchoun, B., Ben Khalifa, A., Mahjoub, M.A., Abu-Ghazaleh, N., Alouani, I. (2023). Jedi: Entropy-based localization and removal of adversarial patches. *Proceedings of the IEEE/CVF Conference on Computer Vision and Pattern Recognition (CVPR)*.

Thys, S., Van Ranst, W., Goedeme, T. (2019). Fooling automated surveillance cameras: Adversarial patches to attack person detection. *Proceedings of the IEEE/CVF Conference on Computer Vision and Pattern Recognition (CVPR) Workshops*.

Tian, Z., Shen, C., Chen, H., He, T. (2019). FCOS: Fully convolutional one-stage object detection. *Proceedings of the IEEE/CVF International Conference on Computer Vision (ICCV)*.

Wang, D., Li, C., Wen, S., Han, Q.-L., Nepal, S., Zhang, X., Xiang, Y. (2021). Daedalus: Breaking nonmaximum suppression in object detection via adversarial examples. *IEEE Transactions on Cybernetics*, 52(8), 7427–7440,

Wang, Y., Tan, Y.-a., Zhang, W., Zhao, Y., Kuang, X. (2020). An adversarial attack on DNN-based black-box object detectors. *Journal of Network and Computer Applications*, 161, 102634,

Wei, X., Liang, S., Chen, N., Cao, X. (2019). Transferable adversarial attacks for image and video object detection. *Proceedings of the Twenty-Eighth International Joint Conference on Artificial Intelligence (IJCAI)*.

Wu, S., Dai, T., Xia, S.-T. (2020). DPAttack: Diffused patch attacks against universal object detection. *arXiv preprint arXiv:2010.11679*, ,

Wu, Z., Lim, S.-N., Davis, L.S., Goldstein, T. (2020). Making an invisibility cloak: Real world adversarial attacks on object detectors. *European Conference on Computer Vision (ECCV)*.

Xia, G.-S., Bai, X., Ding, J., Zhu, Z., Belongie, S., Luo, J., ... Zhang, L. (2018). DOTA: A large-scale dataset for object detection in aerial images. *Proceedings of the IEEE/CVF Conference on Computer Vision and Pattern Recognition (CVPR)*.

Xiang, C., & Mittal, P. (2021). DetectorGuard: Provably securing object detectors against localized patch hiding attacks. *Proceedings of the 2021 ACM SIGSAC conference on computer and communications security*.

Xiang, C., Valtchanov, A., Mahloujifar, S., Mittal, P. (2023). ObjectSeeker: Certifiably robust object detection against patch hiding attacks via patch-agnostic masking. *2023 IEEE Symposium on Security and Privacy (SP)*.

Xie, C., Wang, J., Zhang, Z., Zhou, Y., Xie, L., Yuille, A. (2017). Adversarial examples for semantic segmentation and object detection. *Proceedings of the IEEE International Conference on Computer Vision (ICCV)*.

Xu, K., Zhang, G., Liu, S., Fan, Q., Sun, M., Chen, H., ... Lin, X. (2020). Adversarial T-shirt! Evading person detectors in a physical world. *European Conference on Computer Vision (ECCV)*.

Yahn, Z., Tekin, S.F., Ilhan, F., Hu, S., Huang, T., Xu, Y., ... Liu, L. (2025). Adversarial attention perturbations for large object detection transformers. *Proceedings of the IEEE/CVF International Conference on Computer Vision (ICCV)*.

Yang, C., Huang, Z., Wang, N. (2022). QueryDet: Cascaded sparse query for accelerating high-resolution small object detection. *Proceedings of the IEEE/CVF Conference on Computer Vision and Pattern Recognition (CVPR)*.

Yang, D.Y., Xiong, J., Li, X., Yan, X., Raiti, J., Wang, Y., ... Zhong, Z. (2018). Building towards "Invisible Cloak": Robust physical adversarial attack on YOLO object detector. *2018 9th IEEE Annual Ubiquitous Computing, Electronics & Mobile Communication Conference (UEMCON)*.

Yin, M., Li, S., Song, C., Asif, M.S., Roy-Chowdhury, A.K., Krishnamurthy, S.V. (2022). ADC: Adversarial attacks against object detection that evade context consistency checks. *Proceedings of the IEEE/CVF Winter Conference on Applications of Computer Vision (WACV)*.

Zhang, H., Li, F., Liu, S., Zhang, L., Su, H., Zhu, J., ... Shum, H.-Y. (2023). DINO: DETR with improved denoising anchor boxes for end-to-end object detection. *The Eleventh International Conference on Learning Representations (ICLR)*.

Zhang, H., & Wang, J. (2019). Towards adversarially robust object detection. *Proceedings of the IEEE/CVF International Conference on Computer Vision (ICCV)*.

Zhang, H., Yu, Y., Jiao, J., Xing, E., El Ghaoui, L., Jordan, M. (2019). Theoretically principled trade-off between robustness and accuracy. *International conference on machine learning (ICML)*.

Zhang, H., Zhou, W., Li, H. (2020). Contextual adversarial attacks for object detection. *2020 IEEE international conference on multimedia and expo (ICME)*.

Zhang, R., Isola, P., Efros, A.A., Shechtman, E., Wang, O. (2018). The unreasonable effectiveness of deep features as a perceptual metric. *Proceedings of the IEEE/CVF Conference on Computer Vision and Pattern Recognition (CVPR)*.

Zhang, Y., Zhu, Z., Su, H., Zhu, J., Zheng, S., He, Y., Xue, H. (2023). To make yourself invisible with Adversarial Semantic Contours. *Computer Vision and Image Understanding*, 230, 103659,

Zhao, Y., Zhu, H., Liang, R., Shen, Q., Zhang, S., Chen, K. (2019). Seeing isn't Believing: Towards more robust adversarial attack against real world object detectors. *Proceedings of the 2019 ACM SIGSAC Conference on Computer and Communications Security*.

Zhou, L., Liu, Q., Zhou, S. (2023). Preprocessing-based adversarial defense for object detection via feature filtration. *Proceedings of the 7th International Conference on Algorithms, Computing and Systems*.

Zhu, X., Su, W., Lu, L., Li, B., Wang, X., Dai, J. (2021). Deformable DETR: Deformable transformers for end-to-end object detection. *International Conference on Learning Representations (ICLR)*.